Exploring Phytochemical Composition, Antioxidant, Anti-ESKAPE, Anti-Inflammatory, Anti-α-Amylase Inhibitory Potential of *Rhanterium epapposum* Oliv.: Implications for Phytotherapy

Mejdi Snoussi * and Ahmed Mohajja Alshammari

Posted Date: 14 May 2026

doi: 10.20944/preprints202605.0978.v1

Keywords: *Rhanterium epapposum* Oliv.; anti-ESKAPE; antioxidant; anti-inflammatory; enzymatic assays; in-silico approaches

 doi:10.20944/preprints202605.0978.v1

Article

Exploring Phytochemical Composition, Antioxidant, Anti-ESKAPE, Anti-Inflammatory, Anti-α-Amylase Inhibitory Potential of *Rhanterium epapposum* Oliv.: Implications for Phytotherapy

Mejdi Snoussi * and Ahmed Mohajja Alshammari

Department of Biology. College of Science. University of Hail. P.O. Box 2440. Ha'il 2440. Saudi Arabia

* Correspondence: m.snoussi@uoh.edu.sa

Abstract

Background/Objectives: *Rhanterium epapposum* Oliv. a medicinally valuable plant traditionally used by indigenous communities to treat skin and gastrointestinal ailments and as a natural insecticide, was investigated for its phytochemical composition and diverse biological activities (antioxidant, antimicrobial, anti-inflammatory), and enzyme inhibitory (α-amylase and lipoxygenase), supported by advanced in silico analyses. **Methods:** Methanolic and aqueous extracts were analyzed for total phenolic, flavonoid, and tannin contents, with their metabolite profiles characterized via LC-ESI-MS/MS. Both extracts were comprehensively assessed for antioxidant, antimicrobial, anti-inflammatory, and enzyme inhibitory (α-amylase and 5-lipoxygenase) activities. Furthermore, in silico framework was applied to elucidate the binding efficiency and inhibitory potential of key bioactive compounds against selected pharmacological targets. **Results:** Many bioactive compounds, mainly chlorogenic and syringic acids were identified in both extracts. The aqueous extract showed higher TTC (69.61 ± 0.212 mg TAE/g extract) and TFC (23.81 ± 0.163 mg QE/g extract), while the methanolic extract was richer in phenolics and exhibited overall stronger scavenging antioxidant activity with IC_{50} of 14.9 ± 4.7 µg/mL (DPPH) and 35.0 ± 0.67 µg/mL (ABTS), respectively. both extracts exhibited remarkable antimicrobial activity towards ESKAPE and *Candida* spp. strains. Furthermore, the aqueous extract demonstrated greater, dose-dependent oedema inhibition, peaking at 100 mg/kg, and stronger α-amylase (IC_{50} = 188 µg/mL) and lipoxygenase (IC_{50} = 49 µg/mL) inhibition than the methanolic extract (IC_{50} = 247 µg/mL and 188 µg/mL, respectively), though both were less potent than standard drugs. Molecular docking, MD simulations, and DFT analyses assessed phytocompounds against multiple targets. Chlorogenic acid exhibited multi-target activity, forming hydrogen bonds with Ser49, Thr121, Leu5, Ala7, Asp27 (3FYV), Asp120, Asp86, Asp218 (3Q70), Ser602, Arg415, Asn382, Arg483, Ile461, Ser508 (7Q6S), Gly249, Asp212, Tyr2 (1B2Y), and Gly249, Leu211, Asp212 (1N8Q). MD confirmed complex stability, while DFT (6-31G**) highlighted favorable electronic reactivity and stability. **Conclusions:** Overall, the aqueous and methanolic extracts showed complementary bioactivities, emphasizing their potential as natural therapeutic agents and viable candidates for developing new pharmacological formulations.

Keywords: *Rhanterium epapposum* Oliv.; anti-ESKAPE; antioxidant; anti-inflammatory; enzymatic assays; in-silico approaches

1. Introduction

Noncommunicable diseases (NCDs), including diabetes, cardiovascular disorders, stroke, cancer, and neurodegenerative conditions, are multifactorial chronic disorders that remain among the foremost global causes of disability, morbidity, and mortality [1–3]. These conditions increase the vulnerability of patients to opportunistic and multidrug-resistant infections (caused by clinical multi-

 doi:10.20944/preprints202605.0978.v1

drug-resistant bacteria), especially infections caused by ESKAPE pathogens, which contribute to the development of drug resistance [4,5]. The coexistence of chronic diseases and antimicrobial resistance (AMR) worsen disease severity by exacerbating the situation and constitutes a significant public health concern [6,7]. Moreover, NCDs are closely linked to chronic, dysregulated inflammation [8,9]. As known, inflammation is a protective immune response against external insults and harmful stimuli; however, when it becomes persistent or dysfunctional, it can cause tissue damage and becomes the driving force to the progression of major chronic disorders [10,11]. This situation may also subtly impair metabolic and immune functions, further promoting the development of NCDs [12]. The World Health Organization reports that in 2021 these diseases claimed over 43 million lives, accounting for nearly 75% of non-pandemic-related deaths worldwide and constitute a growing global pandemic with escalating incidence rates [13]. Conventional therapies often constrained by significant limitations, due to their serious side effects, high costs, and limited long-term efficacy, highlighting the pressing demand for safer and more effective options, owing to their capacity to simultaneously influence multiple pathological pathways [14–16].

Accordingly, traditional herbal medicine (THM), as a source of plant-based remedies, has long been practiced across diverse cultures for the treatment of numerous ailments [17–19]. Various plant organs, including leaves, flowers, stems, roots, and fruits (peel and pulp) provide rich reservoirs of biologically active compounds, which can be obtained through different extracts [20–25]. Among them, polyphenols, stand out as key bioactive constituents with multiple pharmacological properties [26–29]. These phytochemicals mitigate oxidative stress and constitute a strategic reservoir for the discovery and development of novel pharmaceutical agents, offering safer, multi-targeted, and biologically effective alternatives for integrative healthcare interventions, particularly in combating chronic diseases [30,31]. Owing to their broad pharmacological activities, plant-derived natural compounds can prevent or attenuate the progression of complex disorders such as diabetes, cardiovascular diseases, cancer, and neurodegenerative conditions [32–37].

R. epapposum, belonging to the Asteraceae family and commonly known as “Arfaj”, is a perennial dwarf shrub plant extensively distributed across Arabian Peninsula, mainly in Saudi Arabia (in northern region) [38]. The plant demonstrates exceptional adaptability to harsh desert conditions, successfully growing in sandy and gravelly loam soils. In folk medicine, it has been employed by rural populations as a remedy for skin infections, gastrointestinal disorders, and as a natural insecticide. Preliminary extract studies reported its richness on phenolics, flavonoids, alkaloids, triterpenes, coumarins (scopoletin), tannins and other phytoconstituents, which underpin its antidiarrheal, antimicrobial, antioxidant, and potential anti-inflammatory activities [39–42]. Numerous plants from the Asteraceae family exhibit potent pharmacological activities, including significant hypoglycemic effects, stimulation of insulin secretion, regeneration of damaged pancreatic β-cells, inhibition of carbohydrate-hydrolyzing enzymes, and strong antioxidant protection against oxidative stress [43,44]. The in-silico approach offers a cost-effective and efficient alternative to conventional drug research [45–47]. Structure-based virtual screening based on computational drug discovery, accelerates drug design and discovery by reducing time and cost while providing reliable predictions [48–50]. Complementarily, DFT calculations yield critical insights into molecular geometry, chemical properties, and potential reactive sites.

Consequently, the proposed study aimed to explore the phytochemical contents, the antioxidant, antimicrobial and anti-inflammatory potencies of both aqueous and ethanolic *R. epapposum* and its anti-amylase inhibitory and lipoxygenase enzyme inhibitory effect. Finally, a comprehensive in silico study, combining DFT, molecular docking, and dynamics simulations, was performed to investigate the structural and electronic properties of bioactive compounds, their interactions with key target proteins, and their potential therapeutic efficacy.

2. Materials and Methods

2. 1-Plant Material Sampling and Preparation of Extracts

 doi:10.20944/preprints202605.0978.v1

The flowering aerial parts of *R. epapposum*, locally known as Marar, were harvested from Jubbah city, located west of Mount Umm Sinman (28°02'30.2"N, 40°53'17.5"E; Saudi Arabia) in May 2023 at 4:30 PM. A voucher specimen (AN07) was deposited at the herbarium of the Department of Biology, College of Science, University of Hail, Hail, Kingdom of Saudi Arabia.

2.2. Total Phenols, Tannins, and Flavonoids Estimation

The prepared extracts were screened for total phenolic content using the Folin–Ciocalteu method, as well as for total tannins and total flavonoid contents, following the procedures previously described by Kumar et al. [51], Broadhurst and Jones [52], and Benariba et al. [53], respectively.

2.3. Screening for Phytoconstituents Using LC-ESI-MS/MS Technique

Chromatographic analysis was conducted using an Agilent 1260 Infinity liquid chromatography system coupled to an Agilent 6420 Triple Quadrupole. Separation of phytochemical constituents was achieved on a Poroshell 120 EC-C18 column (100 mm × 4.6 mm, 2.7 μm particle size). LC–ESI–MS/MS measurements were performed according to the analytical protocol reported previously [54,55], with slight optimization.

The mobile phase system, consisting of 0.1% formic acid in water (solvent A) and methanol (solvent B), was selected due to its superior ability to resolve structurally similar isomeric compounds while simultaneously enhancing detection sensitivity for phenolic constituents. The gradient elution program was as follows: 2% B at 0.00–3.00 min, increased to 25% B at 6.00 min, 50% B at 10.00 min, 95% B at 14.00–17.00 min, and returned to 2% B at 17.50 min. The column temperature was maintained at 25°C, with a flow rate of 0.4 mL/min and an injection volume of 2.0 μL. The mass spectrometer was interfaced with the LC system via an electrospray ionization (ESI) source operating in both positive and negative multiple reaction monitoring (MRM) modes. Instrument parameters were set as follows: capillary voltage −3.5 kV, drying gas temperature 300°C, gas flow rate 11 L/min, and nebulizer pressure 40 psi. Compound identification under MRM conditions was achieved by comparing both retention times and characteristic ion transition pairs with those obtained from authentic reference standards.

2.4. Screening of the Biological Activities

2.4.1. Antimicrobial Activities

The effect on bacterial and fungal growth was estimated by the determination of the minimal inhibitory concentration, and minimal bactericidal/fungicidal concentrations using the microdilution assay in 96 well microtiter plates [26,56]. Ten bacterial strains commonly isolated from hospital care units were included in the antibacterial test namely: *P. aeruginosa*, *E. coli*, *K. pneumoniae*, *E. faecalis*, *E. cloacae*, *E. faecium*, *S. epidermidis*, *A. baumannii*, and *S. aureus* MRSA. Two reference strains were also used (*E. coli* ATCC 10536 and *K. pneumoniae* ATCC 13383). The anti-*Candida* spp. activity was tested against four *Candida* species including *C. albicans* ATCC 10231, *C. utilis* ATCC 9295, *C. glabrata* ATCC 90030, and *C. guillermondii* ATCC 6260. The interpretation of results was done by calculating the MBC/MIC and MFC/MIC ratios for all tested microorganisms, and the scheme of Gatsing et al. [57] was used to classify extracts as bacteriostatic/fungistatic (When MBC/MIC and MFC/MIC values were >4), and bactericidal/fungicidal (When MBC/MIC and MFC/MIC values were ≤4). Ampicillin and Amphotericin B were used as reference drugs.

2.4.2. Antioxidant Activities

The antioxidant potential of the extracts obtained from *R. epapposum* was evaluated using three complementary methods: DPPH radical scavenging, ABTS radical scavenging, and β-carotene–linoleic acid bleaching assays [26,58]. Butylated hydroxytoluene (BHT) and ascorbic acid (AA) served as positive controls for comparison.

 doi:10.20944/preprints202605.0978.v1

2.4.3. Anti-Inflammatory Activity

The anti-inflammatory effect of *R. epapposum* extracts was assessed in Swiss mice using xylene-induced ear edema. Treated and control groups were compared by measuring ear thickness, and the percentage inhibition of edema was calculated [59].

2.4.4. Enzymatic assays

2.4.4.1. Anti-α-amylase enzyme

α-Amylase inhibition was measured using a chromogenic method [60], with porcine pancreatic α-amylase (4 U/mL) and 0.5% potato starch in phosphate buffer (pH 6.9) as the substrate.

2.4.4.2. Anti-Lipoxygenase Activity

Anti-lipoxygenase activity was assessed using linoleic acid as the substrate and soybean lipoxygenase (Sigma, USA) as the enzyme, following established protocols [61,62]. Plant extracts (200–800 µg/mL) were dissolved in 0.25 mL of 2 M borate buffer (pH 9.0) and mixed with 0.25 mL of lipoxygenase solution (final concentration 20,000 U/mL). The percentage inhibition of LOX activity was calculated using the following equation (E1):

% Inhibition= ((AC–As)/Ac) x100 (E1); Where AC represents the absorbance of control and as the absorbance of test sample). A dose–response curve was generated to determine the IC_{50} value, defined as the concentration of the test sample required to inhibit 50% of the enzyme activity.

2.5. Molecular Docking

Molecular docking was performed using the Glide module to assess the ligands' binding affinity and interaction profiles against the antibacterial (PDB ID: 3FYV), antifungal (PDB ID: 3Q70), antioxidant (PDB ID: 7Q6S), anti-inflammatory (PDB ID: 5KIR), alpha-amylase (PDB ID: 1B2Y), and lipoxygenase (PDB ID: 1N8Q) targets. The phyto-compounds used in this study were retrieved from the PubChem database in SDF format and processed with LigPrep to generate relevant protonation and tautomeric states (pH 7.0 ± 0.2), possible stereoisomers, and low-energy 3D conformers, followed by energy minimization using the OPLS force field. Target proteins (3FYV, 3Q70, 7Q6S, 5KIR, 1B2Y, 1N8Q) were prepared using the Protein Preparation Wizard, which assigned bond orders, added hydrogens, fixed missing side chains and loops where possible, predicted protonation states (PROPKA at pH 7.0), optimized the hydrogen-bond network, and performed restrained minimization to avoid clashes. Standard precision (SP) docking was performed for the top-ranked ligands to yield more dependable binding postures [63].

2.6. Molecular Dynamic (MD) Simulation

molecular dynamics simulations of chlorogenic acid in complex with 3FYV and 5KIR were performed for 100 ns using Desmond. Each complex was solvated with SPC water in an orthorhombic box with a 10 Å buffer, neutralized and adjusted to 0.15 M NaCl; systems were energy minimized and equilibrated using a short NVT protocol followed by an NPT equilibration. Production runs were carried out in the NPT ensemble at 300 K and 1 atm using a Nose-Hoover thermostat and a Martyna-Tobias-Klein barostat with a 2-fs integration step, and trajectories were recorded for analysis of RMSD, RMSF, hydrogen-bond persistence and overall conformational stability.

2.7. DFT Study

Density functional theory (DFT) calculations were performed on chlorogenic acid using B3LYP/6-31G to optimize geometry and compute frequency. Frontier molecular orbitals (HOMO–LUMO) and global reactivity descriptors, including chemical hardness, softness, and electronegativity, were analyzed to assess its electronic distribution, stability, and reactivity [64].

 doi:10.20944/preprints202605.0978.v1

2.8. Statistical Analysis

All experiments were conducted in triplicate, and mean values were analyzed using SPSS 20.0 and GraphPad Prism 8.0. Statistical differences were assessed by one-way ANOVA followed by Tukey's post hoc test, with significance set at $p \leq 0.05$.

3. Results

3.1. Characterization of Phenolic Compounds Using LC-ESI-MS/MS

Plant metabolites, spanning diverse chemical classes, exhibit remarkable pharmacological potential, particularly through their anti-inflammatory and enzyme-inhibitory activities, underscoring their therapeutic relevance. In this study, the secondary metabolites of aqueous and methanolic *R. epapposum* extracts (Table 1) were quantified using qualitative and quantitative of LC-ESI-MS/MS technique to elucidate their phenolic acids and flavonoids. Their screening allowed the identification of a total of 17 compounds in both extracts in which chlorogenic acid (4568.77 and 2720.45 µg/g extract) being the prevailing one, followed by syringic acid (799.76 and 1126.68 µg/g extract) in methanolic and water extracts, respectively. Besides, caffeic acid (267.99 µg/g extract), 2,5-dihydroxybenzoic acid (226.96 µg/g extract), protocatechuic acid (231.82 µg/g extract), pyrocatechol (214.66 µg/g extract), ferulic acid (144.37 µg/g extract) and hyperoside (131.46 µg/g extract) were found in high proportions in methanolic extract, while water extract is abundantly by protocatechuic acid (495.84 µg/g extract), 2,5-dihydroxybenzoic (470.20 µg/g extract), and acid pyrocatechol (425.74 µg/g extract).

Table 1. Phytochemical profiling of both aqueous and 80%-methanolic extracts from *R. epapposum* plant species collected from Hail region by using ESI–MS/MS technique.

Identified Compounds	Retention Time (min)	Abondance (mg/Kg of Extract)		Chemical Formula	Molecular Weight (g/mol)
		Aqueous	80%-methanol		
Gallic acid	7.91	34.00±2.32	7.55±0.33	$C_7H_6O_5$	170.12
Pyrocatechol	207.49	425.74±19.21	214.66±8.81	$C_6H_6O_2$	110.11
2,5-Dihydroxybenzoic acid	225.80	470.20±5.12	226.96±1.28	$C_7H_6O_4$	154.12
Protocatechuic acid	231.49	495.84±3.77	231.82±0.36	$C_7H_6O_4$	154.12
3,4-Dihydroxyphenylacetic acid	7.24	24.18±1.05	7.52±0.53	$C_8H_8O_4$	168.14
Chlorogenic acid	4577.29	2720.45±32.64	4568.77±7.37	$C_{16}H_{18}O_9$	354.31
3-Hydroxybenzoic acid	33.91	205.15±0.75	33.83±0.40	$C_7H_6O_3$	138.12
4-Hydroxybenzoic acid	35.20	198.36±6.64	34.08±2.08	$C_7H_6O_3$	138.12
Caffeic acid	267.36	235.23±2.75	267.99±3.27	$C_9H_8O_4$	180.16
Syringic acid	797.06	1126.68±7.26	799.76±5.49	$C_9H_{10}O_5$	198.17
Vanillin	54.11	75.96±1.35	53.23±1.28	$C_8H_8O_3$	152.15
p-Coumaric acid	2.73	64.77±1.70	2.80±0.22	$C_9H_8O_3$	164.16
Ferulic acid	143.49	125.04±3.92	144.37±1.59	$C_{10}H_{10}O_4$	194.18
Hesperidin	17.64	4.13±0.38	17.94±0.27	$C_{28}H_{34}O_{15}$	610.6
Hyperoside	128.19	37.98±1.52	131.46±2.91	$C_{21}H_{20}O_{12}$	464.4
Quercetin	2.19	9.32±0.39	2.38±0.29	$C_{15}H_{10}O_7$	302.23

3.2. Total Phenolics and Antioxidant Activity

In this study, the phenolic contents and antioxidant activity of water and methanol extracts are reported in Table 2. In general, both extracts (aqueous and methanolic) exhibited statistically similar total phenolic contents (TPC) of 24.54 ± 0.122 mg GAE/g extract and 23.68 ± 0.086 mg GAE/g extract, respectively ($p > 0.05$). However, their total flavonoid (TFC) and total tannin contents (TTC) differed

 doi:10.20944/preprints202605.0978.v1

significantly ($p < 0.05$). The TFC values were 22.10 ± 1.670 mg QE/g extract for the aqueous extract and 23.81 ± 0.163 mg QE/g extract for the methanolic extract, while the methanolic extract exhibited a markedly higher TTC (69.61 ± 0.212 mg TAE/g extract), which was approximately 12.5-fold greater than that of the aqueous extract (5.50 ± 0.248 mg TAE/g extract).

Plant materials contain diverse bioactive molecules, and no single method can fully evaluate their antioxidant potential; thus, multiple assays are often required. Among these, phenolic compounds are a key natural antioxidant, valued for both food preservation and protection against oxidative stress–related diseases, making them a central focus in the search for alternatives to synthetic antioxidants. In this context, the antioxidant potential of *R. epapposum* has been evaluated against three methods including, DPPH, ABTS, and β-carotene. The obtained results (Table 2) showed that methanolic extract displayed higher ($p < 0.05$) efficiency in scavenging DPPH and ABTS with respective IC50 values of 14.9 ± 4.7 µg/mL and 35.0 ± 0.67 µg/mL than the aqueous extract (IC50 33.0 ± 4.8 µg/mL and 128.0 ± 0.19 µg/mL), comparable to the reference substances ascorbic (IC50 22.00 ± 0.50 and 21.00 ± 1.00 µg/mL) acid and BHT (IC_{50} 23.00 ± 0.30 and 18.00 ± 0.40 µg/mL). In addition, the β-carotene bleaching test is based on the reaction of β-carotene with peroxyl radicals, generating β-carotene epoxides that act as radical scavengers, and its antioxidant ability can be determined by measuring the inhibition of crocin bleaching. As shown in Table 1, the aqueous extract had significantly ($p < 0.05$) higher potency than the methanolic extract with IC_{50} values of 26.0 ± 4.4 µg/mL and 49.0 ± 1.9 µg/mL, while that of ascorbic acid and BHT remains 17.0 ± 1.0 µg/mL and 42.0 ± 3.5 µg/mL respectively.

Table 2. Antioxidant activities of aqueous/80%-methanolic extracts of *R. epapposum* as compared to standard molecules (Ascorbic acid and butylated hydroxytoluene). Results are reported as the Mean±SD of three experiments. Different letters indicate mean values significantly different at $p < 0.05$, according to a one-way ANOVA followed by Tukey's post hoc test.

Assays	80%-methanolic extract	Aqueous extract	Ascorbic Acid	BHT
Total phenols content (mg GAE/ g extract)	24.54 ± 0.122^{A}	23.68 ± 0.086^{A}	-	-
Total tannins content (mg TAE/ g extract)	5.50 ± 0.248^{C}	69.61 ± 0.212^{B}	-	-
Total flavonoids content (mg QE/ g extract)	22.10 ± 1.670^{B}	23.81 ± 0.163^{A}	-	-
DPPH IC_{50} (µg/mL)	14.9 ± 4.7^{b}	33.0 ± 4.8^{a}	22.0 ± 0.50^{b}	23.0 ± 0.30^{b}
ABTS IC_{50} (µg/mL)	35.0 ± 0.67^{c}	128.0 ± 0.19^{d}	21.0 ± 1.0^{b}	18.0 ± 0.40^{a}
β-carotene IC_{50} (µg/mL)	49.0 ± 1.9^{d}	26.0 ± 4.4^{b}	17.0 ± 1.0^{a}	42.0 ± 3.5^{c}

3.3.1. Pearson Correlation Analysis

As can be seen from the correlated data presented in Table 3, a significant positive correlation was observed between TPC and TTC ($r = 1.000$, $p < 0.01$), *R. epapposum* aqueous extract suggesting that TTC represent a major fraction of the overall polyphenolic compounds, while TFC was significantly high correlated with TFC and TTC ($r = -1.000$, $p < 0.01$). Table revealed a significantly higher positive correlation ($r = 1.000$, $p < 0.01$) between TPC and TTC vs. DPPH and ABTS, and TFC vs. β-carotene, whereas a high negative correlation ($r = -1.000$, $p < 0.01$) was identified for TFC vs. DPPH and ABTS, and TPC and TFC vs. β-carotene β-carotene with $r = 0.93$ and $r = 0.65$, respectively ($p < 0.01$). Conversely, in methanolic *R. epapposum* extract (Table 4), results indicate a strong positive correlation between TPC and TFC ($r = 1.000$, $p < 0.01$), however TTC displayed a weak negative correlation with TPC and TFC ($r = -0.397$, $p < 0.01$) suggesting that the higher the total tannins content, the lower the TFC and TPC. Moreover, ABTS showed a strong negative correlation with TPC and TFC ($r = -1.000$, $p < 0.01$), whereas TPC and TFC were strongly correlated with DPPH and β-carotene

 doi:10.20944/preprints202605.0978.v1

(r = −1.000, p < 0.01). In contrast, TTC displayed a weak negative correlation with DPPH and β-carotene (r = −-0.397, p< 0.01), but a positive correlation with ABTS (r = 0.397, p< 0.01).

Table 3. Pearson's Correlation *R. epapposum* aqueous extract.

	ABTS	DPPH	β-carotene	Phenols	Tannins	Flavonoids
ABTS	1					
DPPH	1.000**	1				
β-carotene	-1.000**	-1.000**	1			
Phenols	1.000**	1.000**	-1.000**	1		
Tannins	1.000**	1.000**	-1.000**	1.000**	1	
Flavonoids	-1.000**	-1.000**	1.000**	-1.000**	-1.000**	1

Significance: **: Correlation is significant at the 0.01 level (2-tailed).

Table 4. Pearson's Correlation of *R. epapposum* 80%-methanolic extract.

	ABTS	DPPH	β-carotene	Phenols	Tannins	Flavonoids
ABTS	1					
DPPH	-1.000**	1				
β-carotene	-1.000**	1.000**	1			
Phenols	-1.000**	1.000**	1.000**	1		
Tannins	0.397	-0.397	-0.397	-0.397	1	
Flavonoids	-1.000**	1.000**	1.000**	1.000**	-0.397	1

Significance: **: Correlation is significant at the 0.01 level (2-tailed).

3.4. Antimicrobial Activity

The antimicrobial activity of both extracts was assessed using broth microdilution assay by measuring MIC, MBC, and MFC values against ESKAPE and *Candida* spp. strains. The results depicted in Table 5 shows that both extracts exhibited excellent, and broad-spectrum antimicrobial activity against various strains with MICs values ranging from 0.171–1.171 mg/L and 0.292–1.171 mg/L for bacterial strains and MICs = 0.585 mg/L for yeasts, for methanolic and aqueous extracts, respectively.

Escherichia coli (ATCC 10536) (MIC 0.171 mg/L), followed by *E. cloacae* (M8) (MICs = 0.292 mg/L) and *E. faecium* (M9) (MIC 0.292 mg/L), were the most susceptible strains to the methanolic extract, while *P. aeruginosa* (M16), *E. cloacae* and *E. faecium* (M9) with MIC value of 0.292 mg/L were the most susceptible strains to the aqueous extract. Ampicillin was used as a standard drug, and its MIC and MBC values ranged from 0.0097 to 2.5 mg/mL and 0.625 to 5 µg/mL.

In addition, *Candida* spp. strains, were similarly inhibited by both extracts. Subsequently, methanolic extract with MBC/MIC ratios of 8-128, exerts bacteriostatic or bacteria-resistant effect, whereas the aqueous extract, with MFC/MIC ratios above 32, showed a *Candida*-resistant strains.

Table 5. Determination of MIC, MBC, and MFC values against ESKAPE and *Candida* spp. strains for both aqueous and 80%-methanolic extracts from *R. epapposum*.

Code	Bacteria tested	*Methanol-80% extract*			*Aqueous extract*			Ampicillin (mg/mL)		
		MIC*	MBC**	MBC/MIC ratio	MIC	MBC	MBC/MIC ratio	MIC	MBC	MBC/MIC ratio
M16	*Pseudomonas aeruginosa*	1.171	9.375	8	0.292	2.343	8	2.5	5	2
M1	*Escherichia coli*	0.585	9.375	16	0.585	9.375	16	0.625	5	8
ATCC 10536	*Escherichia coli*	0.171	18.75	110	0.585	9.375	16	0.0048	1.25	260
M15	*Klebsiella pneumoniae*	0.585	4.687	8	0.585	18.75	32	0.625	5	8

 doi:10.20944/preprints202605.0978.v1

ATCC 13383	*Klebsiella pneumoniae*	0.585	9.375	16	0.585	18.75	32	0.0097	2.5	258
M14	*Klebsiella pneumoniae*	0.585	4.687	8	0.585	18.75	32	0.625	5	8
M7	*Enterococcus faecalis*	1.171	37.5	32	1.171	9.375	8	0.312	2.5	8
M8	*Enterobacter cloacae*	0.292	37.5	128	0.292	37.5	128	0.625	1.25	2
M9	*Enterococcus faecium*	0.292	2.343	8	0.292	37.5	128	0.625	5	8
M13	*Staphylococcus epidermidis*	0.585	4.687	8	0.585	37.5	64	0.312	0.625	2
M17	*Acinetobacter baumannii*	0.585	37.5	64	1.171	75	64	0.019	5	264
M22	*Staphylococcus aureus MRSA*	0.585	37.5	64	1.171	75	64	0.0097	5	516

Code	**Yeast tested**	**Methanol-80% extract**			**Aqueous extract**			**Amphotericin B (mg/mL)**		
		MIC	**MFC***	**MFC/MIC value**	**MIC**	**MFC**	**MFC/MIC ratio**	**MIC**	**MFC**	**MFC/MIC ratio**
ATCC 10231	*Candida albicans*	0.585	37.5	64	0.585	18.75	32	0.195	0.39	2
ATCC 9295	*Candida utilis*	0.585	37.5	64	0.585	37.5	64	0.78	1.56	2
ATCC 90030	*Candida glabrata*	0.585	75.0	128	0.585	18.75	32	0.78	1.56	2
ATCC 6260	*Candida guillermondii*	0.585	75.0	128	0.585	37.5	64	0.097	1.56	16

MIC* : Minimal Inhibitory Concentration expressed in mg/mL ; MBC**: Minimal Bactericidal Concentration expressed in mg/mL; MFC***: Minimal Fungicidal Concentration expressed in mg/mL.

3.5. Anti-Inflammatory Activity

To discover new and safe anti-inflammatory agents, bioactive compounds derived from natural herbs have attracted more attention. In this context, the anti-inflammatory effect of aqueous and methanolic extracts in model rats has been evaluated using the carrageenan-induced ear edema (Figure 1). Dexamethasone was used as a reference drug. A dose-dependent inhibition effect was achieved by both extracts with statistically significant differences between doses and extracts at $p < 0.05$. At low doses (1.56 and 3.12 mg/kg), methanolic extract was inactive to affect edema, however, aqueous extract was effective at these doses inhibiting edema by 43.38% and 60.22% at 1.56 and 3.12 mg/kg, respectively, highlighting the potency of water extract at lower doses. Meanwhile, at the highest dose (100 mg/kg), high suppression of edema by water extract (93.83%), then methanol extract (83.70%) was detected.

 doi:10.20944/preprints202605.0978.v1

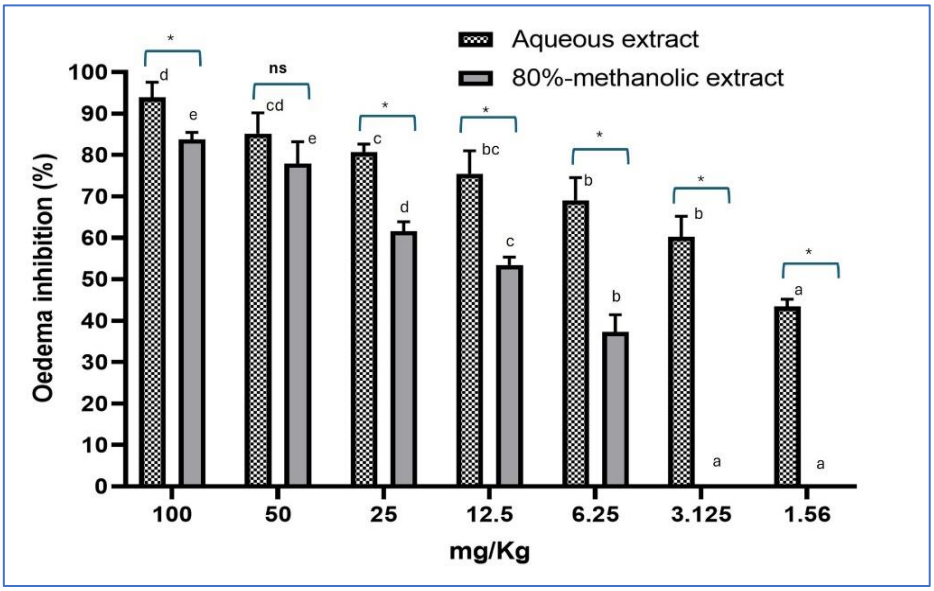

Figure 1. Inhibition of ear edema (%) tested at different concentrations of *R. epapposum* extracts.

3.6. Lipoxygenase/ α-Amylase Inhibitory Activities

Inhibiting the lipoxygenase pathway would prevent leukotriene production and, consequently, could serve as a therapeutic target for treating human inflammation-related diseases. Therefore, the ability of both extracts to treat inflammation was assessed through their potential to inhibit the activity of lipoxygenase. As depicted in Table 6, aqueous extract was a significantly ($p< 0.05$) stronger inhibitor of lipoxygenase (IC50 49 ± 0.82 µg/mL), comparable to Dexamethasone (IC50 36.5±2.07 µg/mL), however methanolic extract showed lesser inhibitory effect with IC50 of 188 ± 6.4 µg/mL, suggesting the potential effect of this plant in managing inflammation.

The management of metabolic disorders can be approached by inhibiting α-amylase, a key digestive enzyme involved in carbohydrate metabolism. Targeting α-amylase by eco-friendly sources as preventive nutraceuticals for drug development remains a promising strategy to reduce glucose absorption and helps prevent postprandial blood sugar spikes, thereby potentially slowing the progression of diabetes. As summarized in Table 6, aqueous extract displayed high potential ability to inhibit α-amylase activity (IC50 188 ± 0.71 µg/mL) than the ethanolic extract (IC50 247 ± 14 µg/mL), but remains lower than the reference drug, acarbose (IC50 247 ± 14 µg/mL).

Table 6. α-Amylase and lipoxygenase assays of aqueous/80%-methanolic extracts of *R. epapposum* as compared to standard molecules (Acarbose and dexamethasone). Results are reported as the Mean±SD of three experiments. Different letters indicate mean values significantly different at $p < 0.05$, according to a one-way ANOVA followed by Tukey's post hoc test.

Assays	α-Amylase (µg/mL)	Lipoxygenase (µg/mL)
Aqueous extract	188±0.71^{b}	49±0.82^{b}
80%-methanolic extract	247±14^{a}	188±6.4^{c}
Acarbose	18.4±0.19^{c}	-
Dexamethasone	-	36.5±2.07^{a}

3.8. In Silico Studies

3.8.1. Molecular Docking

Molecular docking was used to determine the binding ability of phyto-compounds to the specified protein targets (Table 7). The docking scores varied from -2.16 to -8.17 kcal/mol, demonstrating differing affinities across targets. The molecules for the antibacterial protein (PDB ID:

 doi:10.20944/preprints202605.0978.v1

3FYV) have docking scores ranging from -2.16 to -8.17 kcal/mol, with quercetin (-8.17 kcal/mol) appearing as the potential, exceeding the co-crystallized ligand. Scores in the antifungal target (PDB ID: 3Q70) varied from -4.23 to -7.25 kcal/mol, with hesperidin (-7.25 kcal/mol) and hyperoside (-7.09 kcal/mol) exhibiting significant affinities, but still lower than the co-crystallized ligand (-8.95 kcal/mol). The docking scores for the antioxidant target (PDB ID: 7Q6S) varied between -3.02 and -7.59 kcal/mol. Here, quercetin (-7.59 kcal/mol) and luteolin-7-glucoside (-7.04 kcal/mol) exhibited significant binding, although weaker than the co-crystallized ligand (-9.96 kcal/mol). The anti-inflammatory protein (PDB ID: 5KIR) has scores ranging from -5.02 to -7.51 kcal/mol, with hesperidin (-7.51 kcal/mol) and gallic acid (-7.08 kcal/mol) being the most significant similar to the co-crystallized ligand (-9.96 kcal/mol). The docking scores for α-amylase (PDB ID: 1B2Y) were weaker, ranging from -3.28 to -5.62 kcal/mol. The top ligands were 2,5-dihydroxybenzoic acid (-5.62 kcal/mol) and gallic acid (-5.60 kcal/mol), but were less effective than the reference inhibitor (-9.96 kcal/mol). Finally, docking scores for lipoxygenase (PDB ID: 1N8Q) varied from -2.10 to -6.07 kcal/mol, with pyrocatechol (-6.07 kcal/mol) and 4-hydroxybenzoic acid (-5.63 kcal/mol) emerging as the most promising, but less effective than the co-crystallized ligand (-9.96 kcal/mol).

The docking results indicate that the selected phytochemicals engage critical catalytic residues across all six target proteins, suggesting strong inhibitory potential. In the antibacterial target (PDB ID: 3FYV), chlorogenic acid formed hydrogen bonds with Ser49, Thr121, Leu5, Ala7, and Asp27 (Figure 2A), while quercetin interacted with Ser49, Thr121, and Leu5 (Figure 3B). Ser49 and Thr121 are essential for substrate stabilization in the active site, and Asp27 is critical for proton transfer during catalysis. By binding to these residues, both compounds likely obstruct substrate access and inhibit enzymatic activity, with chlorogenic acid providing broader coverage of the catalytic pocket, potentially enhancing antibacterial efficacy.

In the antifungal protein (PDB ID: 3Q70), chlorogenic acid engaged Asp120, Asp86, and Asp218 (Figure 3A), whereas hesperidin interacted with Asp120, Asp218, Gly34, Gly85, and Asn131 (Figure 4B). Asp120 and Asp218 constitute the catalytic dyad responsible for proton transfer, while Gly34 and Gly85 maintain the active site conformation. These interactions suggest that both compounds could interfere with the enzymatic catalytic mechanism, with hesperidin stabilizing the active site through additional hydrogen bonds. For the antioxidant enzyme (PDB ID: 7Q6S), chlorogenic acid formed hydrogen bonds with Ser602, Arg415, Asn382, Arg483, Ile461, and Ser508, and exhibited a π-cation interaction with Arg415 (Figure 4A). Quercetin similarly engaged Arg483, Leu365, Val463, and Arg415 via π-cation interaction (Figure 4B). Arg415 and Ser602 are critical for electron transfer and stabilization of radical intermediates in the catalytic centre. These interactions imply that both compounds may effectively modulate redox activity, with chlorogenic acid forming a more extensive network, enhancing antioxidant potential. In the anti-inflammatory target (PDB ID: 5KIR), chlorogenic acid showed van der Waals interactions with surrounding residues (Figure 5A), whereas quercetin formed hydrogen bonds with Ser530, Gln192, and Phe518 (Figure 5B). Ser530 is a key residue for arachidonic acid binding and COX-2 catalysis. Quercetin's direct engagement with this residue suggests a stronger ability to block prostaglandin synthesis, whereas chlorogenic acid may exert moderate inhibitory effects through stabilization of the surrounding active site environment. Regarding α-amylase (PDB ID: 1B2Y) 2,5-dihydroxybenzoic acid engaged Lys227, Leu211, Gly249, and Asp212 (Figure 6A) while chlorogenic acid formed hydrogen bonds with Gly249, Asp212, and Tyr2 (Figure 6B). Asp212, along with Glu233 and Asp300, constitutes the catalytic triad responsible for glycosidic bond cleavage. The interaction of these phytochemicals with Asp212 and neighbouring residues suggests competitive inhibition at the catalytic site, potentially reducing starch hydrolysis and exhibiting antidiabetic activity. Finally, in lipoxygenase (PDB ID: 1N8Q), chlorogenic acid interacted with Gly249, Leu211, and Asp212 (Figure 7A), while pyrocatechol bound Asp212, Tyr2, and Gly249 (Figure 7B). Asp212 is directly involved in hydrogen abstraction during lipid peroxidation, and Tyr2 contributes to substrate orientation near the iron center. Binding of the phytochemicals to these residues indicates potential inhibition of lipoxygenase-mediated oxidation, which may reduce the formation of pro-inflammatory leukotrienes.

 doi:10.20944/preprints202605.0978.v1

Table 7. Docking scores (kcal/mol) of the phytocompounds against the selected target proteins. The values represent the predicted binding affinities obtained from molecular docking experiments.

Compound	PubChem CID	3FYV	3Q70	7Q6S	5KIR	1B2Y	1N8Q
Gallic acid	370	-6.839	-5.319	-5.492	-7.083	-5.604	-5.625
Pyrocatechol (Catechol)	289	-5.76	-4.712	-4.849	-6.239	-4.975	-6.072
2,5-Dihydroxybenzoic acid	3469	-6.614	-5.675	-5.581	-6.18	-5.623	-5.239
Protocatechuic acid	72	-6.018	-4.909	-5.364	-6.574	-5.419	-5.416
3,4-Dihydroxyphenylacetic acid	547	-5.985	-4.37	-4.345	-6.467	-4.284	-5.596
Chlorogenic acid	1794427	-7.979	-5.852	-3.023	-5.027	-3.534	-2.325
3-Hydroxybenzoic acid	7420	-5.579	-4.996	-5.184	-6.71	-5.125	-5.137
4-Hydroxybenzoic acid	135	-5.748	-4.237	-4.256	-6.233	-4.485	-5.632
Caffeic acid	689043	-6.919	-4.629	-4.742	-6.301	-4.844	-2.621
Syringic acid	10742	-5.52	-5.379	-5.068	-6.565	-4.846	-4.573
Vanillin	1183	-5.242	-4.738	-5.098	-6.319	-4.786	-5.584
p-Coumaric acid	637542	-2.162	-4.536	-4.313	-6.126	-4.128	-5.318
Ferulic acid	445858	-5.506	-4.522	-4.633	-6.815	-4.646	-4.747
Luteolin 7-glucoside	5280637	-5.828	-6.099	-7.046	-5.147	-3.282	-2.324
Hesperidin	10621	-6.918	-7.255	-5.042	-7.517	-4.437	-2.101
Hyperoside	5281643	-7.321	-7.090	-5.266	-5.321	-4.354	-2.678
Quercetin	5280343	-8.172	-5.271	-7.598	-7.083	-4.473	-2.456
Co-crystal ligand	-	-6.955	-8.95	-	-9.969	-	-

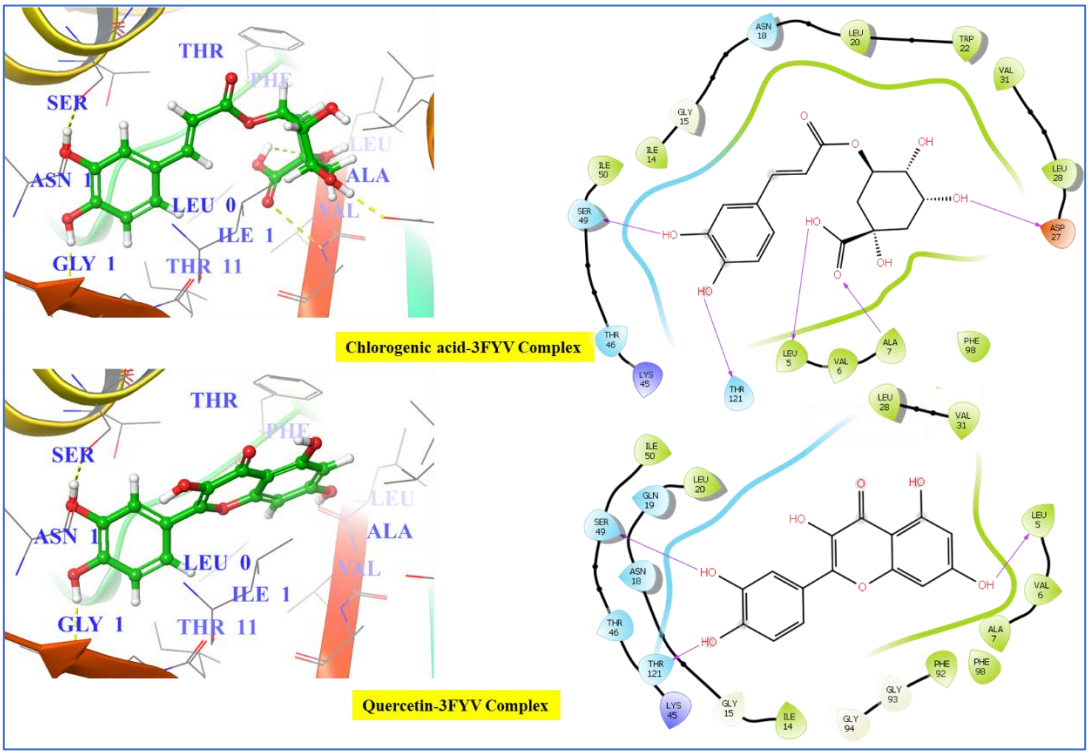

Figure 2. Docking interactions of chlorogenic acid (**A**) and Quercetin (**B**) with *Staphylococcus aureus* enoyl-acyl carrier protein reductase (PDB ID: 3FYV).

Preprints.org (www.preprints.org) | NOT PEER-REVIEWED | Posted: 14 May 2026 doi:10.20944/preprints202605.0978.v1

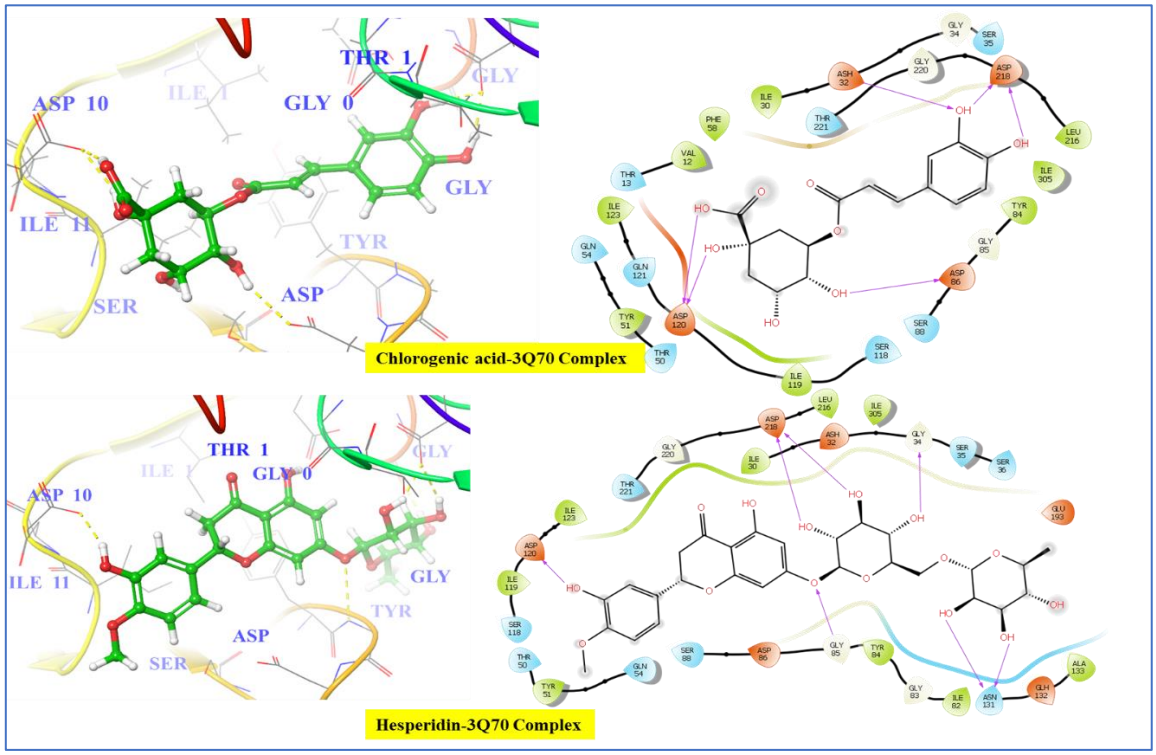

Figure 3. Docking interactions of chlorogenic acid (**A**) and Hesperidin (**B**) with *Candida albicans* dihydrofolate reductase (PDB ID: 3Q70).

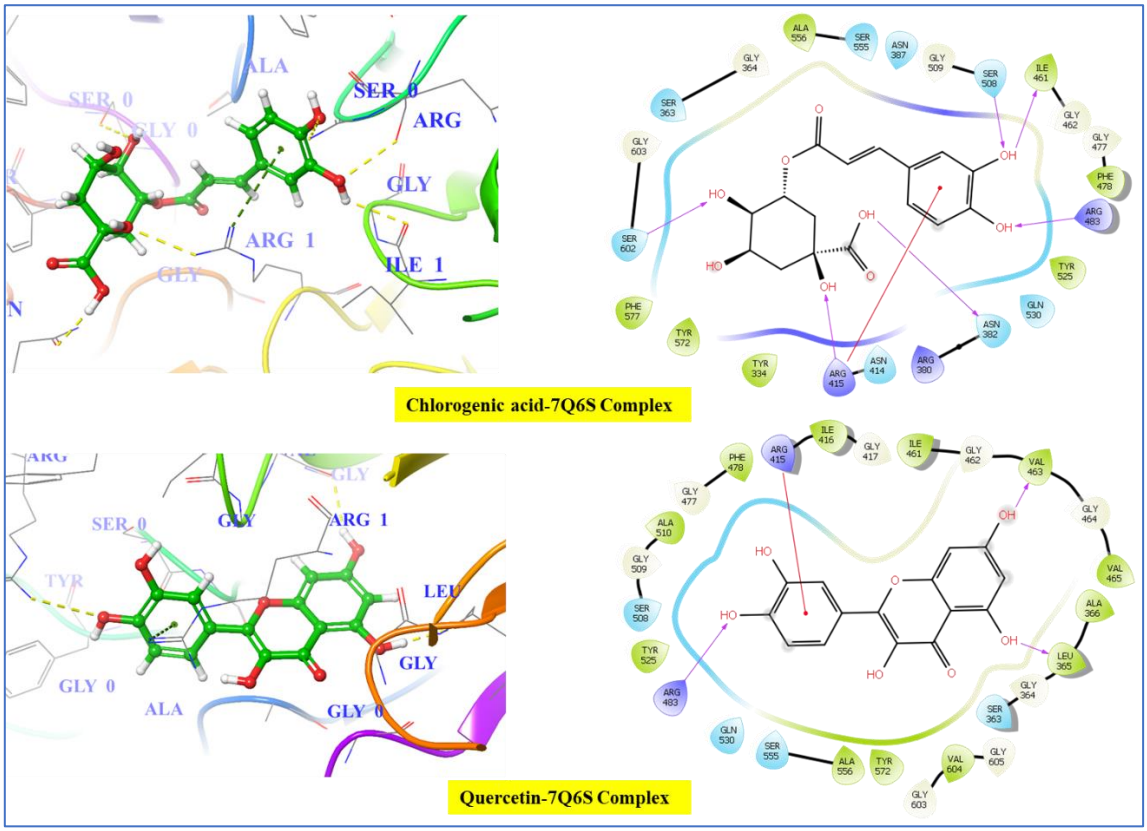

Figure 4. Docking interactions of chlorogenic acid (**A**) and Quercetin (**B**) with Human glutathione peroxidase (PDB ID: 7Q6S).

 doi:10.20944/preprints202605.0978.v1

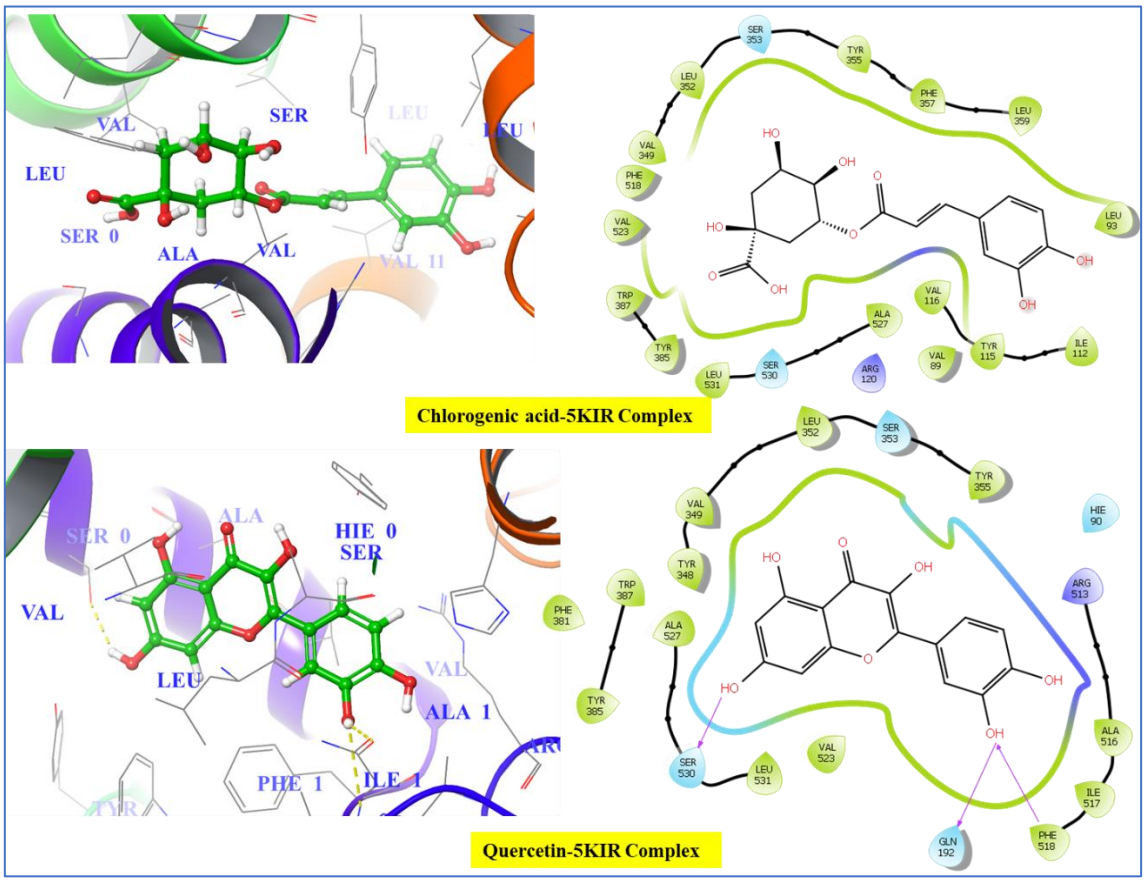

Figure 5. Docking interactions of chlorogenic acid (**A**) and Quercetin (**B**) with Human cyclooxygenase-2 (PDB ID: 5KIR).

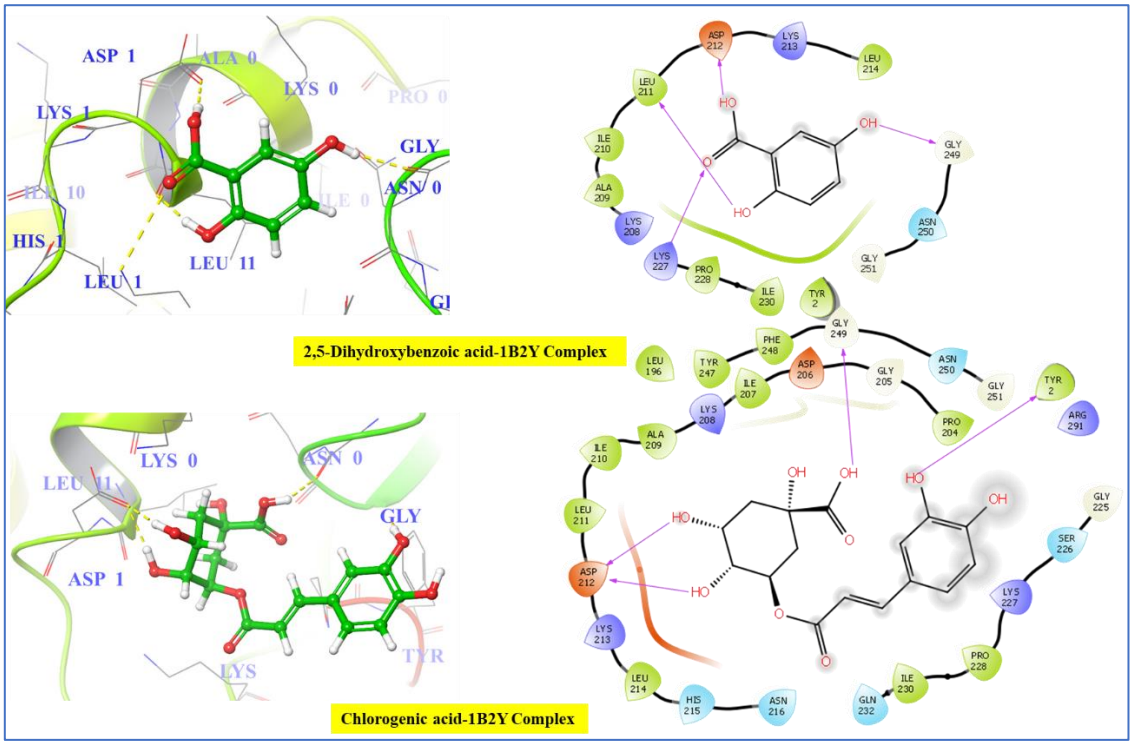

Figure 6. Docking interactions of 2,5-dihydroxybenzoic acid (**A**) and chlorogenic acid (**B**) with Human pancreatic α-amylase (PDB ID: 1B2Y).

Preprints.org (www.preprints.org) | NOT PEER-REVIEWED | Posted: 14 May 2026 doi:10.20944/preprints202605.0978.v1

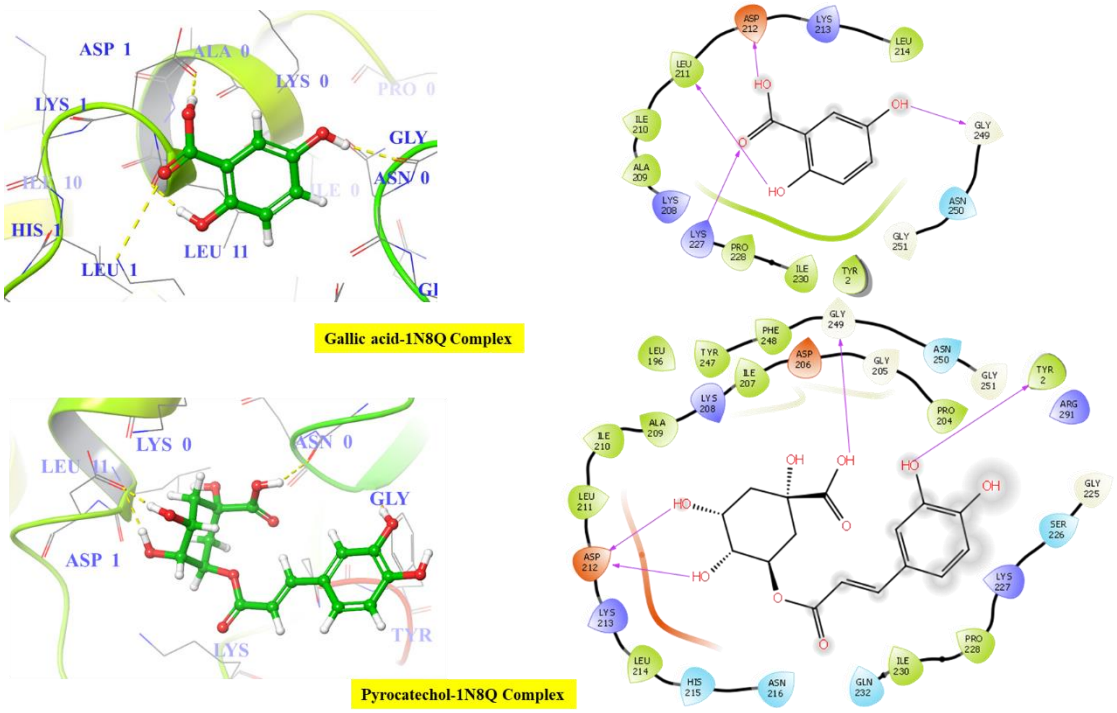

Figure 7. Docking interactions of gallic acid (A) and pyrocatechol (B) with Human 5-lipoxygenase (PDB ID: 1N8Q).

3.8.2. Molecular Dynamic (MD) Simulation

RMSD analysis showed that the chlorogenic acid–5KIR complex displayed a gradual increase in RMSD values up to 28 ns, after which the system reached equilibrium with a mean RMSD of 2.36 Å. In contrast, the chlorogenic acid–3FYV complex achieved stability early in the simulation, maintaining a consistent RMSD throughout with minimal fluctuations. The maximum RMSD for this complex (Figure 8) was 2.36 Å, while the mean RMSD remained lower at 1.77 Å, indicating a highly stable protein–ligand conformation. The 5KIR complex, by comparison, recorded a slightly higher maximum RMSD of 2.97 Å and a mean of 2.30 Å, suggesting minor conformational flexibility but acceptable overall stability.

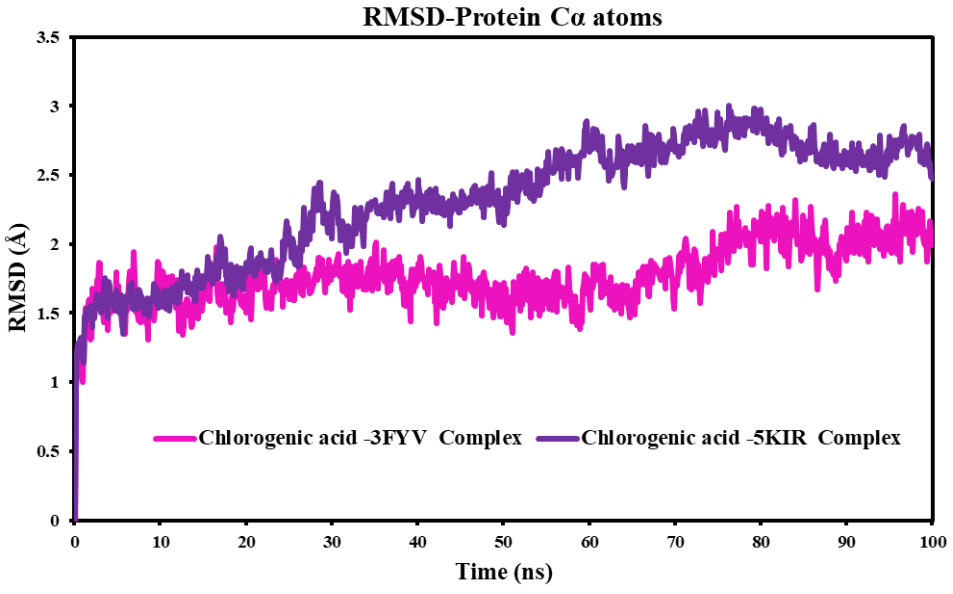

 doi:10.20944/preprints202605.0978.v1

Figure 8. Time-dependent RMSD of protein Cα atoms for Chlorogenic acid–3FYV complex (Indigo) and Chlorogenic acid–5KIR complex (Magenta).

RMSF analysis (Figure 9) further confirmed localized stability within the active site regions of both proteins. The key interacting residues in the chlorogenic acid–3FYV complex included Leu5, Val6, Ala7, Ile14, Gly15, Phe16, Glu17, Asn18, Gln19, Leu20, Trp22, Leu24, Asp27, Lys45, Thr46, Ser49, Ile50, Phe92, Gly94, Gln95, Thr96, Asp120, and Thr121, all of which exhibited minimal fluctuations. Similarly, the chlorogenic acid–5KIR complex involved residues Leu93, Val116, Ser119, Arg120, Val349, Leu352, Ser353, Tyr355, Phe357, Leu359, Leu384, Tyr385, Trp387, Ile517, Phe518, Met522, Val523, Glu524, Ala527, Ser530, Leu531, and Met535, showing consistent atomic stability around the ligand-binding cavity. Hydrogen bond analysis revealed a clear difference between the two systems. The chlorogenic acid–3FYV complex maintained a stronger and more persistent hydrogen bonding network, with a maximum of 7 hydrogen bonds and an average of 3.2, compared to 6 maximum and 2.6 average in the chlorogenic acid–5KIR complex. The hydrogen bonds in the 3FYV system primarily involved Asn18, Phe92, and Asp120, whereas in the 5KIR system, the major interactions were observed with Tyr355, Leu384, and Met522.

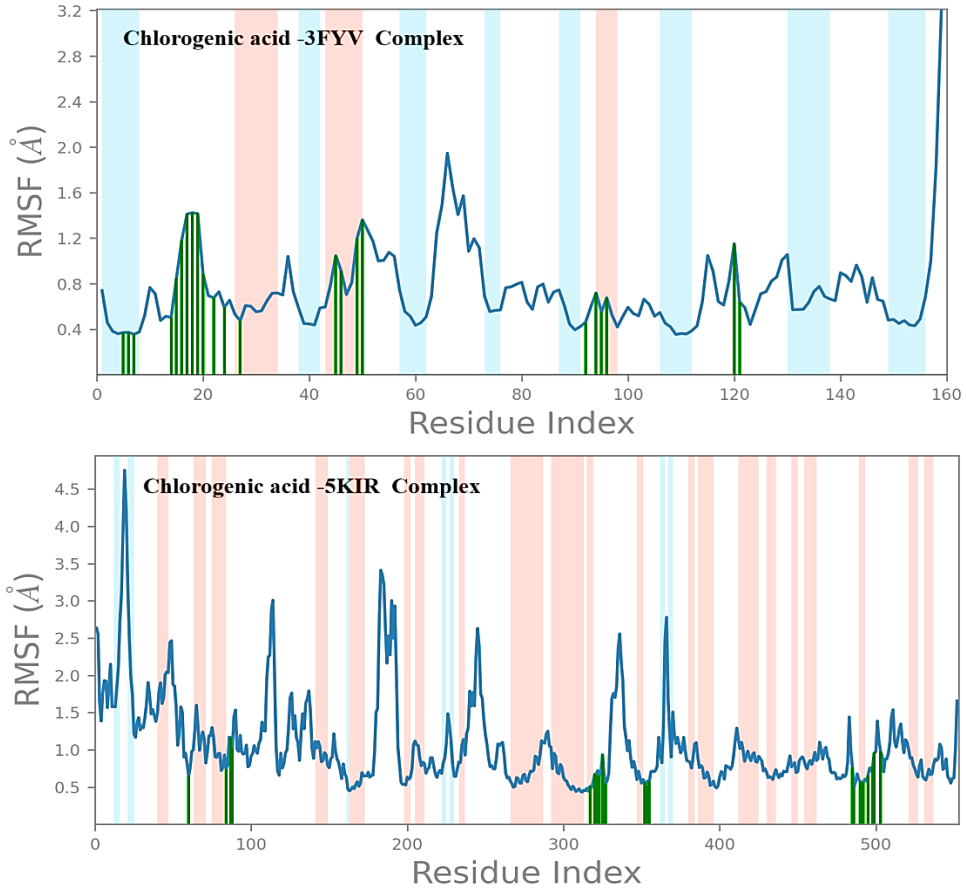

Figure 9. RMSF profile of protein Cα atoms for Chlorogenic acid–3FYV complex (Upper plot) and Chlorogenic acid–5KIR complex (lower plot), showing the residue-wise flexibility throughout the simulation period.

In this study, the chlorogenic acid–3FYV complex exhibited an average RMSD of 1.77 Å, demonstrating remarkable structural stability and limited atomic fluctuation during the 100 ns trajectory. Conversely, the chlorogenic acid–5KIR complex showed a slightly higher average RMSD of 2.30 Å, suggesting minor conformational flexibility (Figure 8). Such moderate deviations are common in proteins with flexible active sites like COX-2 and often reflect adaptive binding, where the active site adjusts slightly to accommodate the ligand. Overall, the RMSD analysis indicates that

 doi:10.20944/preprints202605.0978.v1

both complexes remained dynamically stable, with 3FYV showing superior rigidity and binding retention.

Root Mean Square Fluctuation (RMSF) evaluates the flexibility of individual amino acid residues, highlighting local motions that may influence ligand binding and catalytic activity. 11-12 In the chlorogenic acid–3FYV complex, the interacting residues- Leu5, Val6, Ala7, Ile14, Gly15, Phe16, Glu17, Asn18, Gln19, Leu20, Trp22, Leu24, Asp27, Lys45, Thr46, Ser49, Ile50, Phe92, Gly94, Gln95, Thr96, Asp120, and Thr121 displayed minimal fluctuations, confirming a tightly bound conformation. The reduced motion within these regions suggests that the active-site residues provide a stable hydrophobic and hydrogen bonding environment, effectively anchoring chlorogenic acid. In the 5KIR complex, residues Leu93, Val116, Ser119, Arg120, Val349, Leu352, Ser353, Tyr355, Phe357, Leu359, Leu384, Tyr385, Trp387, Ile517, Phe518, Met522, Val523, Glu524, Ala527, Ser530, Leu531, and Met535 also showed restricted mobility, consistent with their known roles in COX-2 inhibitor binding (Figure 10).

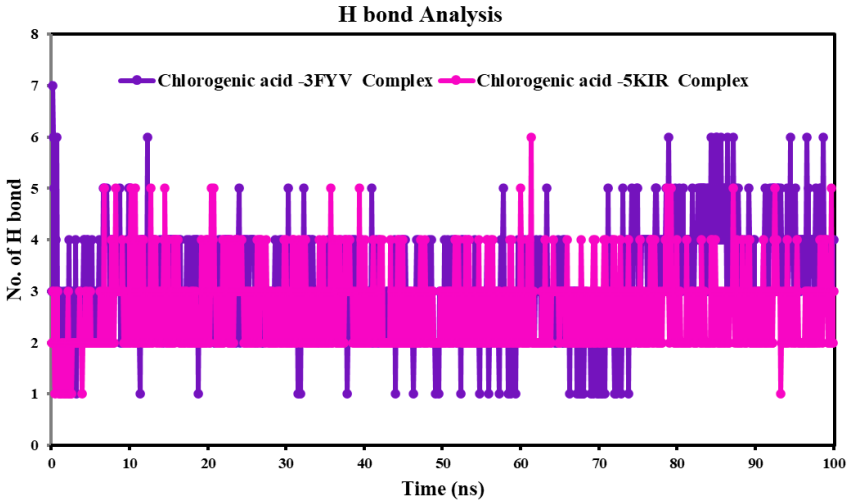

Figure 10. Hydrogen bond analysis of Chlorogenic acid–3FYV complex (Indigo) and Chlorogenic acid–5KIR complex (Magenta), representing the number and stability of hydrogen bonds formed during the simulation.

3.8.3. DFT Study

Table 8 summarizes the results of a DFT study on chlorogenic acid performed with the 6-31G** basis set. The analysis yielded a narrow frontier orbital energy gap of 0.156 eV, derived from HOMO and LUMO energies of -0.212 eV and -0.056 eV, respectively. This small gap suggests a highly reactive molecule, a conclusion supported by related descriptors including a low chemical hardness (η = 0.078 eV) and a high electrophilic index (ω = 0.116 eV).

Table 8. DFT-Based Frontier Molecular Orbital Energies (eV) and Global Reactivity Parameters of Chlorogenic acid.

Code	Chlorogenic acid
HOMO	-0.212
LUMO	-0.056
ΔE	0.156
Ionization potential (IP)	0.212
Electron affinity (EA)	0.056
electronegativity (X)	0.134
Chemical hardness (η)	0.078
Chemical softness (S)	6.412
Chemical potential (μ)	-0.134
Electrophilic index (ω)	0.116

 doi:10.20944/preprints202605.0978.v1

Ionization potential (IP); Electron affinity (EA); electronegativity (X); Chemical hardness (η); Chemical softness (S); Chemical potential (μ); Electrophilic index (ω).

Spatially, the electron-donating HOMO was primarily located on the dihydroxyphenyl moiety, whereas the electron-accepting LUMO extended over both the dihydroxyphenyl and acryloyl segments (Figure 11).

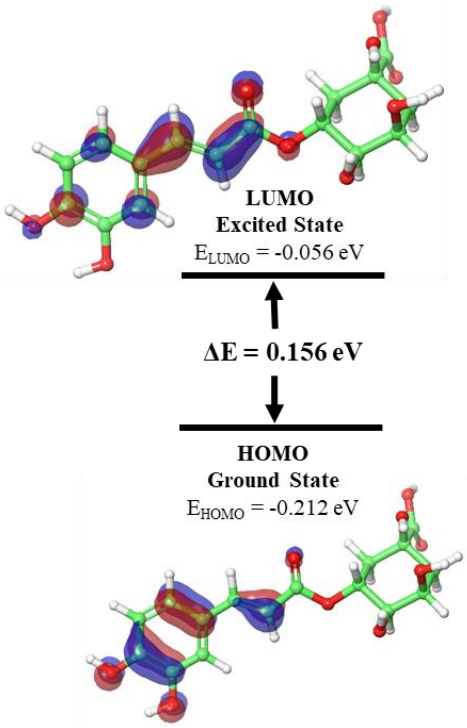

Figure 11. HOMO and LUMO distributions of chlorogenic acid.

4. Discussion

Plants of the Asteraceae family are widely recognized for their therapeutic potential, particularly in the management of oxidative stress, inflammation, and diabetes [65–67]. Among them, *R. epapposum* (the focus of this study) has attracted increasing attention due to its rich profile of bioactive compounds that may contribute to its pharmacological activities. However, only a few fragmented and incomplete studies have previously investigated *R. epapposum*. Interestingly, our findings demonstrated a higher concentration of TCT in water extract measuring 69.61±0.212 mg TAE/ g extract, when compared to that of methanolic extract found at 5.50±0.248 mg TAE/ g extract. In fact, the high content of total condensed tannins (TTC), primarily composed of polyphenolic oligomers, in the water extract can be attributed to their strong polarity and high molecular weight, which favor extraction by the more polar water. In contrast, methanol preferentially extracts low- to medium-molecular-weight phenolics, resulting in a lower TTC. The antioxidant activity of the extracts appears to correlate with their phytochemical contents. Indeed, the aqueous extract, with a very high TTC (69.61 mg TAE/g), effective in preventing lipid peroxidation, exhibited the strongest β-carotene scavenging activity (IC_{50} = 26.0 μg/mL), reflecting the potent activity of high-molecular-weight tannins in lipid-based systems [68]. The antioxidant capacity of tannins increases with the number of hydroxyl groups, which facilitates their oxidation [69,70]. Conversely, the better scavenging ability of methanolic extract with high DPPH (IC_{50} = 14.9 μg/mL vs. 33.0 μg/mL) and ABTS scavenging (IC_{50} = 35.0 μg/mL vs. 128.0 μg/mL), because ethanol can dissolve both polar and less polar antioxidants, unlike water which dissolve only polar molecules [70,71].

Consistent with our findings validated in this study, previous reports have demonstrated that chlorogenic acid, also known as 5-O-caffeoylquinic acid, was found as the major compound in both

 doi:10.20944/preprints202605.0978.v1

R. epapposum extracts, has been widely proven to be well distributed among Asteraceae plants [72–74]. chlorogenic acid has been reported to have a favorable safety profile and good human tolerance [75]. The anti-inflammatory mechanisms of chlorogenic acid involve multiple pathways. It attenuates pathogen-activated NF-κB, JNK, ERK, and p38-MAPK signaling, thereby suppressing the transcription and production of pro-inflammatory mediators [76–81]. Also, it mitigates TNF-α-induced inflammation and OS in 3T3-L1 pre-adipocytes by inhibiting signaling cascades that drive inflammatory and oxidative responses [76,82]. Chlorogenic acid act as inhibitor of α-amylase activity, including porcine pancreatic α-amylase (PPA) isoforms PPA-I and PPA-II. By modulating carbohydrate digestion, it may help to reduce postprandial glucose levels. Additionally, CGA has been shown to enhance insulin secretion from pancreatic β-cells and the islets of Langerhans in rats, suggesting a dual role in both inhibiting carbohydrate hydrolysis and promoting insulin-mediated glucose regulation can competitively inhibit α-amylase activity, including porcine pancreatic α-amylase (PPA) isoforms PPA-I and PPA-II [83–85]. By modulating carbohydrate digestion, CGA may help reduce postprandial glucose levels. Additionally, chlorogenic acid has been shown to enhance insulin secretion from pancreatic β-cells and the islets of Langerhans in rats, suggesting a dual role in both inhibiting carbohydrate hydrolysis and promoting insulin-mediated glucose regulation [86,87].

Syringic acid, as the second major compound found in both *R. epapposum* extracts, is an hydroxybenzoic acid derivative, which also has been identified in several Asteraceae species, including *Achillea millefolium* L., and *Helichrysum arenarium* L. (immortelle) [88]. It is well-known for its strong antioxidant and anti-inflammatory effects, which help alleviate oxidative stress and regulate inflammatory pathways [89]. Zhao et al. [90] discussed the anti-inflammatory mechanisms of syringic acid in detail and concluded that it holds significant therapeutic potential in mitigating oxidative stress and inflammation-related diseases.

To explore the dynamic stability and binding behavior of chlorogenic acid within its target proteins, 100 ns MD simulations were performed for the chlorogenic acid–Staphylococcus aureus enoyl-acyl carrier protein reductase (3FYV) and chlorogenic acid–cyclooxygenase-2 (5KIR) complexes. The molecular dynamics simulation offers valuable insights into the stability, flexibility, and binding strength of chlorogenic acid in the active sites of Staphylococcus aureus enoyl-acyl carrier protein reductase (3FYV) and cyclooxygenase-2 (5KIR). Each simulation parameter RMSD, RMSF, and hydrogen bond analysis-provides distinct but complementary information regarding the conformational behavior and strength of the ligand–protein complex. Root Mean Square Deviation (RMSD) is a crucial parameter that reflects the overall structural stability of a protein–ligand complex throughout the simulation. A lower RMSD value indicates that the system remains close to its initial conformation, implying minimal deviation and stable binding.

The limited RMSF values for these key residues indicate that the ligand stabilizes the local environment, potentially hindering the conformational changes necessary for enzyme catalysis. Thus, the RMSF analysis supports the notion that chlorogenic acid effectively stabilizes both bacterial and mammalian target proteins by reducing local flexibility at critical residues.

Hydrogen bond analysis provides direct evidence of binding strength and persistence, which are vital for maintaining complex stability. The chlorogenic acid–3FYV complex demonstrated a stronger and more persistent hydrogen bonding network, with a maximum of 7 and an average of 3.2 hydrogen bonds, (compared to the 5KIR complex, which exhibited a maximum of 6 and an average of 2.6 hydrogen bonds. Hydrogen bonds formed with Asn18, Phe92, and Asp120 in 3FYV contribute significantly to complex stabilization by enhancing electrostatic complementarity and reducing solvent exposure. In the 5KIR system, hydrogen bonding with Tyr355, Leu384, and Met522 stabilizes the ligand near the COX-2 catalytic site, where Tyr355 and Ser530 are recognized anchoring residues for NSAID-type inhibitors. The higher average hydrogen bond occupancy in the 3FYV complex suggests stronger electrostatic interactions and greater conformational rigidity, which could enhance inhibitory efficiency. Taken together, these parameters indicate that chlorogenic acid forms robust and energetically favorable interactions within both targets, though the 3FYV complex

 doi:10.20944/preprints202605.0978.v1

demonstrates higher dynamic stability and stronger bonding. The low RMSD, restricted RMSF fluctuations, and sustained hydrogen bonding collectively support the conclusion that chlorogenic acid is a promising inhibitor with stable conformations against bacterial and inflammatory enzymes.

The ionization potential (0.212 eV) and electron affinity (0.056 eV) confirm the molecule's ability to readily donate and accept electrons, indicating its involvement in redox-related biological activities. The moderate electronegativity (0.134 eV) and negative chemical potential (-0.134 eV) indicate a preference for electron donation rather than withdrawal. Chlorogenic acid has a low chemical hardness (0.078 eV) and a high softness (6.412 eV^{-1}), making it highly reactive and suitable for interactions with biomolecular targets like enzymes and free radicals. The electrophilic index (0.116 eV) reflects its moderate electrophilicity, which may contribute to its ability to interact with nucleophilic residues in proteins. Overall, the DFT results show that the electron-rich dihydroxyphenyl moiety is the primary reactive site, which explains chlorogenic acid's strong antioxidant activity, whereas extended conjugation with the acryloyl group increases its stability and binding potential with biological macromolecules.

5. Conclusions

For the first time, this study integrates phytochemical, biological, and in silico approaches to characterize Rhanterium epapposum Oliv., revealing its strong therapeutic potential. Both aqueous and methanolic extracts, rich in phenolic compounds such as chlorogenic and syringic acids, showed significant antioxidant, antimicrobial, anti-inflammatory, and enzyme inhibitory activities, including effects against ESKAPE pathogens and Candida spp. Computational analyses confirmed multi-target interactions, particularly for chlorogenic acid, supporting the experimental results and highlighting its role as a key bioactive scaffold. Further in vivo studies, compound isolation, and formulation development are needed to support clinical translation. Overall, *R. epapposum* represents a promising natural source for developing new therapies against oxidative stress, infections, inflammation, and metabolic disorders.

Author Contributions: Conceptualization, M.S. and A.M.A.; methodology, M.S. and A.M.A.; software, M.S.; resources, A.M.A.; data curation, A.M.A.; writing—original draft preparation, M.S. and A.M.A.; writing—review and editing, M.S. and A.M.A. All authors have read and agreed to the published version of the manuscript.

Funding: "This research received no external funding".

Institutional Review Board Statement: "Not applicable".

Informed Consent Statement: "Not applicable.".

Data Availability Statement: The original contributions presented in this study are included in the article. Further inquiries can be directed to the corresponding authors.

Conflicts of Interest: "The authors declare no conflicts of interest.".

References

1. Malta, D.C.; Veloso, G.A.; Gomes, C.S.; Barreto, M.L. Noncommunicable chronic diseases and health challenges in 2050. Rev. Bras. Epidemiol. 2026, 29, e260011.
2. Freihat, O.; Sipos, D.; Aamir, M.; Kovacs, A. Global burden and future projections of non-communicable diseases (2000–2050): Progress toward SDG 3.4 and disparities across regions and risk factors. PLoS One 2025, 20(12), e0336036.
3. Khatiwada, B.; Rajbhandari, B.; Mistry, S.K.; Parsekar, S.; Yadav, U.N. Prevalence of and factors associated with health literacy among people with noncommunicable diseases (NCDs) in South Asian countries: A systematic review. Clin. Epidemiol. Glob. Health 2022, 101174.

 doi:10.20944/preprints202605.0978.v1

4. Mulani, M.S.; Kamble, E.E.; Kumkar, S.N.; Tawre, M.S.; Pardesi, K.R. Emerging strategies to combat ESKAPE pathogens in the era of antimicrobial resistance: A review. Front. Microbiol. 2019, 10, 539.
5. Aldarhami, A.; Bazaid, A.S.; Alhamed, A.S.; Alghaith, A.F.; Ahamad, S.R.; Alassmrry, Y.A.; Alharazi, T.; Snoussi, M.; Qanash, H.; Alamri, A.; Badraoui, R.; Kadri, A.; Binsaleh, N.K.; Alreshidi, M. Antimicrobial potential of Pithecellobium dulce seed extract against pathogenic bacteria: In silico and in vitro evaluation. Biomed. Res. Int. 2023, 2023, 2848198.
6. Abdul-Mutakabbir, J.; Abdul-Mutakabbir, R. Syndemics of antimicrobial resistance: Non-communicable diseases, social deprivation, and the rise of multidrug-resistant infections. Infect. Dis. Ther. 2025, 14, 1561–1575.
7. Venmans, L.M.; Hak, E.; Gorter, K.J.; Rutten, G.E. Incidence and antibiotic prescription rates for common infections in patients with diabetes in primary care over the years 1995 to 2003. Int. J. Infect. Dis. 2009, 13, e344–e351.
8. Yu, X.; Pu, H.; Voss, M. Overview of anti-inflammatory diets and their promising effects on non-communicable diseases. Br. J. Nutr. 2024, 132, 898–918.
9. Padrón-Monedero, A. A pathological convergence theory for non-communicable diseases. Aging Med. 2023, 6, e12273.
10. Cumming, E.; Peters, C. Immune response to infection. Anaesth. Intensive Care Med. 2024, 25, 101491.
11. Gaikwad, V.V.; Gitaje, S.R.; Joshi, S.D.; Kharmate, S.V.; Phalle, D.R.; More, M.P.; Mali, M.A.; Shingade, P.P. Mechanisms of inflammation associated with chronic diseases: A brief review. J. Adv. Med. Med. Res. 2025, 37, 48–56.
12. Phillips, C.M.; Chen, L.-W.; Heude, B.; Bernard, J.-Y.; Harvey, N.C.; Duijts, L.; Mensink-Bout, S.M.; Polanska, K.; Mancano, G.; Suderman, M.; et al. Dietary inflammatory index and non-communicable disease risk: A narrative review. Nutrients 2019, 11, 1873.
13. World Health Organization. Noncommunicable diseases. Available online: https://www.who.int/news-room/fact-sheets/detail/noncommunicable-diseases (accessed on 28 September 2025).
14. Omotayo, O.; Maduka, C.P.; Muonde, M.; Olorunsogo, T.O.; Ogugua, J.O. The rise of non-communicable diseases: A global health review of challenges and prevention strategies. Int. Med. Sci. Res. J. 2024, 4, 74–88.
15. Huang, Y.; Lyu, X.; Kam, Y.W. Therapeutic Vaccines for Non-Communicable Diseases: Global Progress and China's Deployment Pathways. Vaccines (Basel) 2025, 13, 881.
16. Darrow, J.J.; Kesselheim, A.S. A New Wave of Vaccines for Non-Communicable Diseases: What Are the Regulatory Challenges? Food Drug Law J. 2015, 70, 243–258.
17. Zhang, J.; Hu, K.; Di, L.; Wang, P.; Liu, Z.; Zhang, J.; Yue, P.; Song, W.; Zhang, J.; Chen, T.; Wang, Z.; Zhang, Y.; Wang, X.; Zhan, C.; Cheng, Y.-C.; Li, X.; Li, Q.; Fan, J.-Y.; Shen, Y.; Han, J.-Y.; Qiao, H. Traditional herbal medicine and nanomedicine: Converging disciplines to improve therapeutic efficacy and human health. Adv. Drug Deliv. Rev. 2021, 176, 113964.
18. Kropi, K.; Jastone, K.P.; Kharumnuid, S.A.; Kumar Das, H.; Naga, M.M. Cross-cultural study on the uses of traditional herbal medicine to treat various women's health issues in Northeast India. J. Ayurveda Integr. Med. 2024, 15, 101024.
19. Kadri, A. Comprehensive Phytochemical Analysis of Various Plantago albicans Solvent Extracts and Their Potential Antioxidant and Antimicrobial Effects. Biocatal. Agric. Biotechnol. 2023, 52, 102886.
20. Felhi, S.; Hajlaoui, H.; Ncir, M.; Bakari, S.; Ktari, N.; Saoudi, M.; Gharsallah, N.; Kadri, A. Nutritional, phytochemical and antioxidant evaluation and FT-IR analysis of freeze-dried extracts of Ecballium elaterium fruit juice from three localities. Food Science and Technology 2016, 36, 646–655.
21. Kadri, A.; Zarai, Z.; Ben Chobba, I.; Bekir, A.; Gharsallah, N.; Damak, M.; Gdoura, R. Chemical constituents and antioxidant properties of Rosmarinus officinalis L. essential oil cultivated from South-Western Tunisia. Journal of Medicinal Plants Research 2011, 5, 5999–6004.
22. Snoussi, M.; Noumi, E.; Hajlaoui, H.; Bouslama, L.; Hamdi, A.; Saeed, M.; Alreshidi, M.; Adnan, M.; Al-Rashidi, A.; Aouadi, K.; et al. Phytochemical Profiling of Allium subhirsutum L. Aqueous Extract with Antioxidant, Antimicrobial, Antibiofilm, and Anti-Quorum Sensing Properties: In Vitro and In Silico Studies. Plants 2022, 11, 495.

 doi:10.20944/preprints202605.0978.v1

23. Hajlaoui, H.; Arraouadi, S.; Mighri, H.; Chaaibia, M.; Gharsallah, N.; Ros, G.; Nieto, G.; Kadri, A. Phytochemical Constituents and Antioxidant Activity of Oudneya Africana L. Leaves Extracts: Evaluation Effects on Fatty Acids and Proteins Oxidation of Beef Burger during Refrigerated Storage. Antioxidants 2019, 8, 442.
24. Nieto, G.; Martínez-Zamora, L.; Peñalver, R.; Marín-Iniesta, F.; Taboada-Rodríguez, A.; López-Gómez, A.; Martínez-Hernández, G.B. Applications of Plant Bioactive Compounds as Replacers of Synthetic Additives in the Food Industry. Foods 2024, 13, 47.
25. El-Saadony, M.T.; Saad, A.M.; Mohammed, D.M.; Alkafaas, S.S.; Abd El-Mageed, T.A.; Fahmy, M.A.; Ahmed, A.E.; Algopishi, U.B.; Abu-Elsaoud, A.M.; Mosa, W.F.A.; AbuQamar, S.F.; El-Tarabily, K.A. Plant bioactive compounds: Extraction, biological activities, immunological and nutritional aspects, food applications, and human health benefits—A comprehensive review. Frontiers in Nutrition 2025, 12, 1659743.
26. Ciupei, D.; Colişar, A.; Leopold, L.; Stănilă, A.; Diaconeasa, Z.M. Polyphenols: From Classification to Therapeutic Potential and Bioavailability. Foods 2024, 13, 4131.
27. Haddaji, F.; Papetti, A.; Noumi, E.; Ghars, M.; Gharsallah, H.; Snoussi, M.; Aouadi, K.; Kadri, A. Bioactivities and In Silico Study of Pergularia tomentosa L. Phytochemicals as Potent Antimicrobial Agents Targeting Type IIA Topoisomerase, TyrRS, and Sap1 Virulence Proteins. Environmental Science and Pollution Research 2021, 28, 25349–25367.
28. El Mannoubi, I.; Alghamdi, N.M.; Bashir, S.H.; Mohamed, S.A.; Chaabane, H.; Abdalla, A.N.; Abid, S.; Kadri, A.; de Oliveira, M.S. UPLC-ESI-QTOF-MS/MS profiling, antioxidant, and cytotoxicity potentials of Marrubium vulgare L. extracts: Experimental analysis and computational validation. Chemistry & Biodiversity 2025, e00400.
29. Noumi, E.; Ahmad, I.; Adnan, M.; Patel, H.; Merghni, A.; Haddaji, N.; Bouali, N.; Alabbosh, K.F.; Kadri, A.; Caputo, L.; et al. Illicium verum L. essential oil: GC/MS profile, molecular docking study, in silico ADME profiling, quorum sensing, and biofilm-inhibiting effect on foodborne bacteria. Molecules 2023, 28, 7691.
30. Srivastava, V.; Dhiman, V.K.; Pandey, A.; Verma, S.K.; Singh, D. Harnessing the Medicinal Potential of Herbs through Hormesis: Perspectives in Global Health and Therapeutics. Food Chemistry Advances 2025, 7, 101011.
31. Chaachouay, N.; Zidane, L. Plant-Derived Natural Products: A Source for Drug Discovery and Development. Drugs Drug Candidates 2024, 3, 184–207.
32. Kang, K.S. Phytochemical Constituents of Medicinal Plants for the Treatment of Chronic Inflammation. Biomolecules 2021, 11, 672.
33. Naik, R.A.; Rajpoot, R.; Koiri, R.K.; Bhardwaj, R.; Aldairi, A.F.; Johargy, A.K.; Faidah, H.; Babalghith, A.O.; Hjazi, A.; Alsanie, W.F.; Alamri, A.S.; Alhomrani, M.; Alsharif, A.; Shkodina, A.; Singh, S.K. Dietary Supplementation and the Role of Phytochemicals against Alzheimer's Disease: Focus on Polyphenolic Compounds. J. Prev. Alzheimers Dis. 2025, 12(1), 100004.
34. Piccialli, I.; Tedeschi, V.; Caputo, L.; D'Errico, S.; Ciccone, R.; De Feo, V.; Secondo, A.; Pannaccione, A. Exploring the Therapeutic Potential of Phytochemicals in Alzheimer's Disease: Focus on Polyphenols and Monoterpenes. Front. Pharmacol. 2022.
35. Mahmud, A.R.; Ema, T.I.; Siddiquee, M.F.; et al. Natural flavonols: actions, mechanisms, and potential therapeutic utility for various diseases. Beni-Suef Univ. J. Basic Appl. Sci. 2023, 12, 47.
36. Ghosh, S.; Basu, S.; Kayal, T.; et al. Computational advancements to facilitate therapeutic application of phytochemicals: Where do we stand?. Discov. Appl. Sci. 2025, 7, 491.
37. Dereli-Caliskan, N.; Husunet, M.; Ila, H.; Karagoz, I. Determination of potential anti-Alzheimer activity of gentiopicroside and isoorientin using molecular docking studies. Eurasia Proc. Sci. Technol. Eng. Math. 2021, 12, 106–112.
38. Collenette, S. Wild Flowers of Saudi Arabia; National Commission for Wildlife Conservation and Development (NCWCD): Riyadh, Saudi Arabia; East Anglian Engraving Co. Ltd.: Norwich, UK, 1999; p. 213.

 doi:10.20944/preprints202605.0978.v1

39. Shama, I.Y.; Shama, I.Y.; Adam, S.E. Comparative Toxicity of Trichodesma africanum and Rhanterium epapposum Aerial Parts Aqueous and Methanolic Extracts on Wistar Rats. J. Pharmacol. Toxicol. 2012, 7(3), 128–139.
40. Rajendrasozhan, S.; Moll, H.E.; Snoussi, M.; Romeilah, R.M.; Shalaby, E.A.; Younes, K.M.; El-Beltagi, H.S. Phytochemical Screening and Antimicrobial Activity of Various Extracts of Aerial Parts of Rhanterium epapposum. Processes 2021, 9, 1351.
41. El-Ashmawy, I.M.; Aljohani, A.S.M.; Soliman, A.S. Studying the Bioactive Components and Phytochemicals of the Methanol Extract of Rhanterium epapposum Oliv.. Appl. Biochem. Biotechnol. 2024, 196, 2414–2424.
42. Alanazi, A.D.; Alghabban, A.J. Antileishmanial and Synergic Effects of Rhanterium epapposum Essential Oil and Its Main Compounds Alone and Combined with Glucantime against Leishmania major Infection. Int. J. Parasitol. Drugs Drug Resist. 2024, 26, 100571.
43. Rolnik, A.; Olas, B. The Plants of the Asteraceae Family as Agents in the Protection of Human Health. Int. J. Mol. Sci. 2021, 22, 3009.
44. Mohanta, Y.K.; Mishra, A.K.; Nongbet, A.; Chakrabartty, I.; Mahanta, S.; Sarma, B.; Panda, J.; Panda, S.K. Potential Use of the Asteraceae Family as a Cure for Diabetes: A Review of Ethnopharmacology to Modern-Day Drug and Nutraceutical Developments. Front. Pharmacol. 2023, 14, 1153600.
45. Noumi, E.; Ahmad, I.; Bouali, N.; Patel, H.; Ghannay, S.; Alrashidi, A.A.; Abdulhakeem, M.A.; Patel, M.; Ceylan, O.; Badraoui, R.; et al. Thymus musilii Velen. Methanolic Extract: In Vitro and In Silico Screening of Its Antimicrobial, Antioxidant, Anti-Quorum Sensing, Antibiofilm, and Anticancer Activities. Life 2023, 13, 62.
46. Bouali, N.; Hammouda, M.B.; Ahmad, I.; Ghannay, S.; Thouri, A.; Dbeibia, A.; Patel, H.; Hamadou, W.S.; Hosni, K.; Snoussi, M.; et al. Multifunctional Derivatives of Spiropyrrolidine Tethered Indeno-Quinoxaline Heterocyclic Hybrids as Potent Antimicrobial, Antioxidant and Antidiabetic Agents: Design, Synthesis, In Vitro and In Silico Approaches. Molecules 2022, 27, 7248.
47. El Yaqoubi, M.; Lahyaoui, M.; Mazzah, A.; El-Idrissi, H.; Seqqat, Y.; Haoudi, A.; Sghyar, R.; Saffaj, T.; Ihssane, B.; Ouazzani Chahdi, F.; Kandri Rodi, Y. An integrated computational approach combining QSAR modeling, molecular docking, and ADME profiling for the discovery of selective CYP11B1 inhibitors. Sci. Afr. 2026, 31, e03176.
48. Adeyi, A.O.; Afolayan, F.I.D.; Salaam, R.A.; Ajisebiola, B.S.; Adeyi, E.O.; Ajala, O.T.; Okonji, R.E. Computational identification of potential inhibitors for dominant proteins in Viperidae snakes from FDA-approved drugs. Sci. Afr. 2026, 31, e03215.
49. Othman, I.M.M.; Gad-Elkareem, M.A.M.; Anouar, E.; Aouadi, K.; Snoussi, M.; Kadri, A. New Substituted Pyrazolones and Dipyrazolotriazines as Promising Tyrosyl-tRNA Synthetase and Peroxiredoxin-5 Inhibitors: Design, Synthesis, Molecular Docking and Structure-Activity Relationship (SAR) Analysis. Bioorg. Chem. 2021, 109, 104704.
50. Isah, J.J.; Uzairu, A.; Uba, S.; Ibrahim, M.T. Machine learning–driven discovery and optimization of PI3Kδ inhibitors for diffuse large B-cell lymphoma. Sci. Afr. 2026, 31, e03206.
51. Kumar, M.; Gupta, V.; Kumari, P.; Reddy, C.; Jha, B. Assessment of Nutrient Composition and Antioxidant Potential of Caulerpaceae Seaweeds. J. Food Compos. Anal. 2011, 24, 270–278.
52. Broadhurst, R.B.; Jones, W.T. Analysis of Condensed Tannins Using Acidified Vanillin. J. Sci. Food Agric. 1978, 29, 788–794.
53. Benariba, N.; Djaziri, R.; Bellakhdar, W.; Belkacem, N.; Kadiata, M.; Malaisse, W. Phytochemical Screening and Free Radical Scavenging Activity of Citrullus colocynthis Seeds Extract. Asian Pac. J. Trop. Biomed. 2013, 3, 35–40.
54. Cittan, M.; Çelik, A. Development and Validation of an Analytical Methodology Based on Liquid Chromatography–Electrospray Tandem Mass Spectrometry for the Simultaneous Determination of Phenolic Compounds in Olive Leaf Extract. J. Chromatogr. Sci. 2018, 56, 336–343.
55. Khalfaoui, A.; Noumi, E.; Belaabed, S.; Aouadi, K.; Lamjed, B.; Adnan, M.; Defant, A.; Kadri, A.; Snoussi, M.; Khan, M.A.; et al. LC-ESI/MS-Phytochemical Profiling with Antioxidant, Antibacterial, Antifungal,

 doi:10.20944/preprints202605.0978.v1

Antiviral and In Silico Pharmacological Properties of Algerian Asphodelus tenuifolius (Cav.) Organic Extracts. Antioxidants 2021, 10, 628.

56. Ghannay, S.; Aouadi, K.; Kadri, A.; Snoussi, M. In Vitro and In Silico Screening of Anti-Vibrio spp., Antibiofilm, Antioxidant and Anti-Quorum Sensing Activities of Cuminum cyminum L. Volatile Oil. Plants 2022, 11, 2236.
57. Gatsing, D.; Tchakoute, V.; Ngamga, D.; Kuiate, J.-R.; Tamokou, J.D.D.; Nji-Nkah, B.F.; Tchouanguep, F.M.; Fodouop, S.P.C. In Vitro Antibacterial Activity of Crinum purpurascens Herb. Leaf Extract against the Salmonella Species Causing Typhoid Fever and Its Toxicological Evaluation. Iran. J. Med. Sci. 2009, 34, 126–136.
58. Hamdi, A.; Viaene, J.; Mahjoub, M.A.; Majouli, K.; Gad, M.H.H.; Kharbach, M.; Demeyer, K.; Marzouk, Z.; Vander Heyden, Y. Polyphenolic contents, antioxidant activities and UPLC–ESI–MS analysis of Haplophyllum tuberculatum A. Juss leaves extracts. Int. J. Biol. Macromol. 2018, 106, 1071–1079.
59. Abdelhamid, A.; Jouini, M.; Bel Haj Amor, H.; Mzoughi, Z.; Dridi, M.; Ben Said, R.; Bouraoui, A. Phytochemical Analysis and Evaluation of the Antioxidant, Anti-Inflammatory, and Antinociceptive Potential of Phlorotannin-Rich Fractions from Three Mediterranean Brown Seaweeds. Mar. Biotechnol. 2018, 20, 60–74.
60. Chokki, M.; Cudălbeanu, M.; Zongo, C.; Dah-Nouvlessounon, D.; Ghinea, I.O.; Furdui, B.; Raclea, R.; Savadogo, A.; Baba-Moussa, L.; Avamescu, S.M.; Dinica, R.M.; Baba-Moussa, F. Exploring Antioxidant and Enzyme (α-Amylase and β-Glucosidase) Inhibitory Activity of Morinda lucida and Momordica charantia Leaves. Foods 2020, 9, 434.
61. 61-Nile, S.H.; Nile, A.; Oh, J.-W.; Kai, G. Soybean Processing Waste: Potential Antioxidant, Cytotoxic and Enzyme Inhibitory Activities. Food Biosci. 2020, 38, 100778. http://dx.doi.org/10.1016/j.fbio.2020.100778
62. 62-Eshwarappa, R.S.B.; Ramachandra, Y.L.; Subaramaihha, S.R.; Subbaiah, S.G.P.; Austin, R.S.; Dhananjaya, B.L. Anti-Lipoxygenase Activity of Leaf Gall Extracts of Terminalia chebula (Gaertn.) Retz.(Combretaceae). Pharmacogn. Res. 2016, 8, 78. http://dx.doi.org/10.4103/0974-8490.175574
63. 63-Ghosh, S., Das, S., Ahmad, I., & Patel, H. (2021). In silico validation of anti-viral drugs obtained from marine sources as a potential target against SARS-CoV-2 Mpro. Journal of the Indian Chemical Society, 98(12), 100272. https://doi.org/10.1016/j.jics.2021.100272
64. 64- Chaudhari, B.; Patel, H.; Thakar, S.; Ahmad, I.; Bansode, D. Optimizing Sunitinib for Cardiotoxicity and Thyrotoxicity by a Scaffold Hopping Approach. In Silico Pharmacol. 2022, 10(1), 10. https://doi.org/10.1007/s40203-022-00125-1
65. 65- Arulselvan, P.; Tangestani Fard, M.; Tan, W.S.; Gothai, S.; Fakurazi, S.; Norhaizan, M.E.; Kumar, S.S. Role of Antioxidants and Natural Products in Inflammation. Oxid. Med. Cell. Longev. 2016, 2016, 5276130. https://doi.org/10.1155/2016/5276130
66. 66- Rolnik, A.; Olas, B. The Plants of the Asteraceae Family as Agents in the Protection of Human Health. Int. J. Mol. Sci. 2021, 22(6), 3009. https://doi.org/10.3390/ijms22063009
67. 67- Carvalho, A. R. Jr.; Diniz, R. M.; Suarez, M. A. M.; Figueiredo, C. S. S. e S.; Zagmignan, A.; Grisotto, M. A. G.; Fernandes, E. S.; da Silva, L. C. N. Use of Some Asteraceae Plants for the Treatment of Wounds: From Ethnopharmacological Studies to Scientific Evidences. Front. Pharmacol. 2018, 9, 784. https://doi.org/10.3389/fphar.2018.00784
68. 68- Gülçin L, Huyut Z, Elmasta M, Aboul-Enein HY. Radical scavenging and antioxidant activity of tannic acid. Arab J Chem. (2010) 3:43–53. doi: 10.1016/j.arabjc.2009.12.008
69. 69- Tong, Z.; He, W.; Fan, X.; Guo, A. Biological Function of Plant Tannin and Its Application in Animal Health. Front. Vet. Sci. 2021, 8, 803657. https://doi.org/10.3389/fvets.2021.803657
70. 70- Olejar KJ, Ray S, Kilmartin PA. Enhanced antioxidant activity of polyolefin films integrated with grape tannins. J Sci Food Agric. (2016) 96:2825–31. doi: 10.1002/jsfa.7450
71. Gulcin, İ.; Alwasel, S.H. DPPH Radical Scavenging Assay. Processes 2023, 11, 2248.
72. Ko, M.J.; Nam, H.H.; Chung, M.S. Subcritical water extraction of bioactive compounds from Orostachys japonicus A. Berger (Crassulaceae). Sci. Rep. 2020, 10, 10890.
73. Garcia-Perez, P.; Garcia-Oliveira, P.; Finimundy, T.C.; Pinela, J.; Calhelha, R.C.; Nenadić, M.; Soković, M.; Simal-Gandara, J.; Barros, L.; Prieto, M.A. Authenticity and Bioactive Markers Search in the Phenolic-Rich

 doi:10.20944/preprints202605.0978.v1

Extracts of Asteraceae Medicinal Plants Through Integrative Computational Chemometrics. Food Sci. Nutr. 2025, 13, 4720.

74. Fraisse, D.; Felgines, C.; Texier, O.; Jean-Louis, J. Caffeoyl Derivatives: Major Antioxidant Compounds of Some Wild Herbs of the Asteraceae Family. Food Nutr. Sci. 2011, 2, 4889.
75. Gupta, A.; Atanasov, A.G.; Li, Y.; Kumar, N.; Bishayee, A. Chlorogenic acid for cancer prevention and therapy: Current status on efficacy and mechanisms of action. Pharmacol. Res. 2022, 186, 106505.
76. Nguyen, V.; Taine, E.G.; Meng, D.; Cui, T.; Tan, W. Chlorogenic Acid: A Systematic Review on the Biological Functions, Mechanistic Actions, and Therapeutic Potentials. Nutrients 2024, 16, 924.
77. Ji, L.; Jiang, P.; Lu, B.; Sheng, Y.; Wang, X.; Wang, Z. Chlorogenic acid, a dietary polyphenol, protects acetaminophen-induced liver injury and its mechanism. J. Nutr. Biochem. 2013, 24, 1911–1919.
78. Hwang, S.J.; Kim, Y.-W.; Park, Y.; Lee, H.-J.; Kim, K.-W. Anti-inflammatory effects of chlorogenic acid in lipopolysaccharide-stimulated RAW 264.7 cells. Inflamm. Res. 2014, 63, 81–90.
79. Shi, H.; Dong, L.; Jiang, J.; Zhao, J.; Zhao, G.; Dang, X.; Lu, X.; Jia, M. Chlorogenic acid reduces liver inflammation and fibrosis through inhibition of toll-like receptor 4 signaling pathway. Toxicology 2013, 303, 107–114.
80. Zheng, Z.; Sheng, Y.; Lu, B.; Ji, L. The therapeutic detoxification of chlorogenic acid against acetaminophen-induced liver injury by ameliorating hepatic inflammation. Chem. Biol. Interact. 2015, 238, 93–101.
81. Krakauer, T. The polyphenol chlorogenic acid inhibits staphylococcal exotoxin-induced inflammatory cytokines and chemokines. Immunopharmacol. Immunotoxicol. 2002, 24, 113–119.
82. Goya, L.; Sánchez-Medina, A.; Redondo-Puente, M.; Dupak, R.; Bravo, L.; Sarriá, B. Main Colonic Metabolites from Coffee Chlorogenic Acid May Counteract Tumor Necrosis Factor-alpha-Induced Inflammation and Oxidative Stress in 3T3-L1 Cells. Molecules 2023, 29, 88.
83. Oboh, G.; Agunloye, O.M.; Adefegha, S.A.; Akinyemi, A.J.; Ademiluyi, A.O. Caffeic and chlorogenic acids inhibit key enzymes linked to type 2 diabetes (in vitro): A comparative study. J. Basic Clin. Physiol. Pharmacol. 2015, 26, 165–170.
84. Pérez-Nájera, V.C.; Gutiérrez-Uribe, J.A.; Antunes-Ricardo, M.; Hidalgo-Figueroa, S.; Del-Toro-Sánchez, C.L.; Salazar-Olivo, L.A.; Lugo-Cervantes, E. Smilax aristolochiifolia Root Extract and Its Compounds Chlorogenic Acid and Astilbin Inhibit the Activity of alpha-Amylase and alpha-Glucosidase Enzymes. Evid. Based Complement. Alternat. Med. 2018, 2018, 6247306.
85. Narita, Y.; Inouye, K. Kinetic analysis and mechanism on the inhibition of chlorogenic acid and its components against porcine pancreas alpha-amylase isozymes I and II. J. Agric. Food Chem. 2009, 57, 9218–9225.
86. Tousch, D.; Lajoix, A.-D.; Hosy, E.; Azay-Milhau, J.; Ferrare, K.; Jahannault, C.; Cros, G.; Petit, P. Chicoric acid, a new compound able to enhance insulin release and glucose uptake. Biochem. Biophys. Res. Commun. 2008, 377, 131–135.
87. Fernandez-Gomez, B.; Ramos, S.; Goya, L.; Mesa, M.D.; del Castillo, M.D.; Martín, M. Coffee silverskin extract improves glucose-stimulated insulin secretion and protects against streptozotocin-induced damage in pancreatic INS-1E beta cells. Food Res. Int. 2016, 89, 1015–1022.
88. Srinivasulu, C.; Ramgopal, M.; Ramanjaneyulu, G.; Anuradha, C.M.; Suresh Kumar, C. Syringic acid (SA) – A review of its occurrence, biosynthesis, pharmacological and industrial importance. Biomed. Pharmacother. 2018, 108, 547–557.
89. Zhao, Z.; Yang, Q.; Sun, Y.; Ruan, X. Unveiling the antioxidant and anti-inflammatory potential of syringic acid: mechanistic insights and pathway interactions. Front. Pharmacol. 2025, 16, 1615294.
90. Sytar, O.; Zivcak, M.; Konate, K.; Brestic, M. Phenolic Acid Patterns in Different Plant Species of Families Asteraceae and Lamiaceae: Possible Phylogenetic Relationships and Potential Molecular Markers. Sci. World J. 2022, 2022, 9632979.